From the Department of Neurobiology, Care Sciences and Society
Karolinska Institutet, Stockholm, Sweden

THE MATTER OF WHITE AND GRAY MATTER IN COGNITIVE IMPAIRMENT

Soheil Damangir

Stockholm 2017

The Matter of White and Gray Matter in Cognitive Impairment

THESIS FOR DOCTORAL DEGREE (Ph.D.)

By

Soheil Damangir

Principal Supervisor:
Dr. Gabriela Spulber
Karolinska Institutet
Department of Neurobiology,
Care Sciences and Society
Division of Clinical Geriatrics

Co-supervisors:
Professor Lars-Olof Wahlund
Karolinska Institutet
Department of Neurobiology,
Care Sciences and Society
Division of Clinical Geriatrics

Dr. Ir. Hugo Vrenken
VU University Medical Center, Amsterdam
Department of Radiology and Nuclear Medicine

Opponent:
Professor Norbert Schuff
University of California San Francisco
School of Medicine
Department of Radiology

Examination Board:
Professor Nancy Pedersen
Karolinska Institutet
Department of Medical Epidemiology and
Biostatistics

Docent Stefan Skare
Karolinska Institutet
Department of Clinical Neuroscience

Professor Rolf A. Heckemann
University of Gothenburg
Sahlgrenska Academy
MedTech West

To my family and friends,

With love

"Intelligence is the ability to avoid doing work, yet getting the work done."

— Linus Torvalds

ABSTRACT

Cognitive impairment spans from minor subjective cognitive impairment to disabling dementia. Many biomarkers have been developed to monitor different aspects of cognitive impairment. Magnetic resonance imaging is the most used neuroimaging biomarker in research and can measure gray matter (GM) and white matter (WM) changes. Although there is a consensus that atrophy in GM is a marker for neuronal loss, there is little evidence assessing the role of WM changes. The aim of this thesis is to first develop a tool to reliably measure the changes in WM in the form of white matter hyperintensities (WMH) and second to evaluate the role of WM and GM changes in the early stages of cognitive decline.

In *Study I* and *Study II*, a fully automated method for segmentation of WMH has been developed and validated. Validation results indicated that the WMH segmentation was performed with high similarity to manual delineation and with superb reproducibility.

In *Study III*, coronary heart disease (CHD) and hypertension, which are known to contribute to WM damage, were examined and their effect on GM and WM changes was investigated on a group of 69 individuals with 30-year follow-up. We showed that CHD and hypertension indeed affect the GM volume and thickness and the effect of CHD is partially independent of hypertension. However, the results indicate no significant effect on WMH, which we believe is due to the fact that WMH were measured as a crude total volume.

In *Study IV*, a pipeline was developed to isolate the WM tract connecting each GM region to the rest of the brain and to measure the burden of WMH on each tract, hereinafter *tract-based WMH*. We used a cohort of 257 cognitively normal (CTL), 87 subjective cognitive impairment (SCI) and 124 mild cognitive impairment (MCI) subjects and examined their GM volume, *tract-based WMH* and cognitive performance. Our results indicated that the fraction of variance in GM volume that can be explained by *tract-based WMH* in SCI subjects is significantly higher than in both CTL and MCI subjects. The results also showed that in subjects with high and low cognitive performance, *tract-based WMH* can barely explain any GM volume change. However, in subjects with slight cognitive impairment *tract-based WMH* can explain the changes in GM volume.

In summary, we investigated different ways of measuring the damage of WMH and showed that the role of WMH is more pronounced when measuring them in relation to the WM tract they affect. The effect of WMH on GM has been shown to be mainly in the earlier stages of cognitive impairment.

LIST OF SCIENTIFIC PAPERS INCLUDED IN THE THESIS

I. **Soheil Damangir**, Amirhossein Manzouri, Ketil Oppedal, Stefan Carlsson, Michael J. Firbank, Hogne Sonnesyn, Ole-Bjørn Tysnes, John T. O'Brien, Mona K. Beyer, Eric Westman, Dag Aarsland, Lars-Olof Wahlund, and Gabriela Spulber, 2012. Multispectral MRI segmentation of age related white matter changes using a cascade of support vector machines. J. Neurol. Sci. 322, 211–216.

II. **Soheil Damangir**, Eric Westman, Andrew Simmons, Hugo Vrenken, Lars-Olof Wahlund, and Gabriela Spulber, 2016. Reproducible Segmentation of White Matter Hyperintensities Using a New Statistical Definition. Magn. Reson. Mater. Physics, Biol. Med. 30, 227–237.

III. Miika Vuorinen, **Soheil Damangir**, Eini Niskanen, Julia Miralbell, Minna Rusanen, Gabriela Spulber, Hilkka Soininen, Miia Kivipelto, and Alina Solomon, 2014. Coronary heart disease and cortical thickness, gray matter and white matter lesion volumes on MRI. PLoS One 9, 1–9.

IV. **Soheil Damangir**, Oskar Hansson, Olof Lindberg, Erik Stomrud, Danielle van Westen, Eric Westman, Hugo Vrenken, Lars-Olof Wahlund and Gabriela Spulber. 2017. The relationship between gray matter atrophy and white matter hyperintensities in anatomically connected tracts in subjects with cognitive impairment. Submitted manuscript

LIST OF SCIENTIFIC PAPERS NOT INCLUDED IN THE THESIS

I.   Keith S. Cover, Ronald A. van Schijndel, Adriaan Versteeg, Kelvin K. Leung, Emma R. Mulder, Remko A. Jong, Peter J. Visser, Alberto Redolfi, Jerome Revillard, Baptiste Grenier, David Manset, **Soheil Damangir**, Paolo Bosco, Hugo Vrenken, Bob W. van Dijk, Giovanni B. Frisoni, and Frederik Barkhof, 2016. Reproducibility of hippocampal atrophy rates measured with manual, FreeSurfer, AdaBoost, FSL/FIRST and the MAPS-HBSI methods in Alzheimer's disease. Psychiatry Res. Neuroimaging 252, 26–35.

II. Miika Vuorinen, Gabriela Spulber, **Soheil Damangir**, Eini Niskanen, Tiia Ngandu, Hilkka Soininen, Miia Kivipelto, and Alina Solomon, 2015. Midlife CAIDE Dementia Risk Score and Dementia-Related Brain Changes up to 30 Years Later on Magnetic Resonance Imaging. J. Alzheimer's Dis. 44, 93–101.

III. Gro O. Nygaard, Sigrid A. De Rodez Benavent, Hanne F. Harbo, Bruno Laeng, Piotr Sowa, **Soheil Damangir**, Kristian Bernhard Nilsen, Lars Etholm, Siren Tønnesen, Emilia Kerty, Liv Drolsum, Nils Inge Landrø, and Elisabeth G. Celius, 2015. Eye and hand motor interactions with the Symbol Digit Modalities Test in early multiple sclerosis. Mult. Scler. Relat. Disord. 4, 585–589.

IV. Piotr Sowa, Atle Bjørnerud, Gro O. Nygaard, **Soheil Damangir**, Gabriela Spulber, Elisabeth G. Celius, Paulina Due-Tønnessen, Hanne F. Harbo, and Mona K. Beyer, 2015. Reduced perfusion in white matter lesions in multiple sclerosis. Eur. J. Radiol. 84, 2605–2612.

V.   Tobias Granberg, Juha Martola, Gösta Bergendal, Sara Shams, **Soheil Damangir**, Peter Aspelin, Sten Fredrikson, and Maria Kristoffersen-Wiberg, 2014. Corpus callosum atrophy is strongly associated with cognitive impairment in multiple sclerosis: Results of a 17-year longitudinal study. Mult. Scler. J. 1151–1158.

VI. Gro O. Nygaard, Kristine B. Walhovd, Piotr Sowa, Joy-Loi Chepkoech, Atle Bjørnerud, Paulina Due-Tønnessen, Nils I. Landrø, **Soheil Damangir**, Gabriela Spulber, Andreas B. Storsve, Mona K. Beyer, Anders M. Fjell, Elisabeth G. Celius, and Hanne F. Harbo, 2014. Cortical thickness and surface area relate to specific symptoms in early relapsing--remitting multiple sclerosis. Mult. Scler. J. 21, 402–414.

VII. Seyed-Mohammad Fereshtehnejad, **Soheil Damangir**, Pavla Cermakova, Dag Aarsland, Maria Eriksdotter, and Dorota Religa, 2014. Comorbidity profile in dementia with Lewy bodies versus Alzheimer's disease: a linkage study between the Swedish Dementia Registry and the Swedish National Patient Registry. Alzheimers. Res. Ther. 6, 1–14.

LIST OF OPEN-SOURCE SOFTWARE DEVELOPED FOR THE THESIS

   I. ***Cascade*** – Reproducible Segmentation of White Matter Changes
      https://github.com/Damangir/Cascade

  II. ***Connectivity*** – Tract Based Measurement of White Matter Damage
      https://github.com/Damangir/Connectivity

 III. ***SSP*** – Simple Pipeline Management System
      https://github.com/Damangir/SSP

CONTENTS

LIST OF ABBREVIATIONS

AD	Alzheimer's Disease
AF	Flip Angle
AQT	A Quick Test of Cognitive Speed
ANOVA	Analysis of Variance
Aβ	Amyloid Beta
BioFINDER	Biomarkers for Identifying Neurodegenerative Disorders Early and Reliably
BET	Brain Extraction Tool
CAIDE	Cardiovascular Risk Factors, Aging and Dementia
CHD	Coronary Heart Disease
CSF	Cerebrospinal Fluid
CT	Computed Tomography
CTL	Cognitively Healthy Control
DA	Axial Diffusivity
DemWest	Dementia Study in Western Norway
DSM-IV	Diagnostic and Statistical Manual for Mental Diagnosis IV
DTI	Diffusion Tensor Imaging
FA	Fractional Anisotropy
FAST	FMRIB's Automated Segmentation Tool
FDG	^{18}Fludeoxyglucose
FLAIR	Fluid-Attenuated Inversion Recovery
FLIRT	FMRIB's Linear Image Registration Tool
FNIRT	FMRIB's Non-linear Image Registration Tool
FSL	FMRIB Software Library
GDP	Gross Domestic Product
GM	Gray Matter
IQR	Interquartile Range
KHP-DCR	Kings Health Partners-Dementia Case Register
LBD	Lewy Body Dementia
LST	Lesion Segmentation Tool
MCI	Mild Cognitive Impairment

MD	Mean Diffusivity
MMSE	Mini–Mental State Examination
MRI	Magnetic Resonance Imaging
MTA	Medial Temporal Lobe Atrophy
PiB	Pittsburgh Compound B
PD	Proton Density
PDD	Parkinson Disease Dementia
PET	Positron Emission Tomography
RD	Radial Diffusivity
ROC	Receiver Operating Characteristic
SCI	Subjective Cognitive Impairment
SD	Standard Deviation
SG	Slice Gap
SPECT	Single-Photon Emission Computed Tomography
ST	Slice Thickness
SVD	Small Vessel Disease
SveDem	Swedish Dementia Registry
SVM	Support Vector Machine
TE	Echo Time
TI	Inversion Time
TOADS	Topology Preserving Anatomical Segmentation
VaD	Vascular Dementia
WM	White Matter
WMH	White Matter Hyperintensities

1 INTRODUCTION

1.1 COGNITIVE IMPAIRMENT

Cognitive impairment is a general term for the condition of decline of mental capabilities. It spans from minor subjective cognitive impairment, to mild cognitive impairment observed objectively all the way to its extreme disabling dementia. Cognitive impairment symptoms vary among individuals but most people with cognitive impairment experience impairment in their memory, language, attention, reasoning or visual perception. It is estimated that more than 46 million people worldwide suffer from dementia [Wimo et al., 2017]. Aging is the greatest known risk factor for cognitive impairment and dementia. Due to the constant increase in the aged population, its burden is expected to increase even more. Currently, there are more than 150,000 people with dementia in Sweden with an enormous health, social and financial burden [Socialstyrelsen, 2014]. The annual financial burden of dementia on the Swedish economy is reported to be 63 billion Swedish kronor [Wimo et al., 2016]. To put this enormous burden into perspective, it is more than the annual operating income of IKEA and AstraZeneca combined or about five times Ericsson's annual operating income (Figure 1). The global cost of dementia was estimated to be US $818 billion in 2015 [Wimo et al., 2017] which exceeds the gross domestic product (GDP) of Sweden and Finland combined [Organisation for Economic Co-operation and Development, 2016].

Figure 1 Annual cost of dementia compared to the operating income of famous companies in Sweden. The cost is equivalent to 1.5 times IKEA's, 3 times AstraZeneca's or 5 times Ericsson's annual operating income.

Cognitive impairment due to neurodegeneration is diagnosed when a person experiences subjective or objective decline from a previous level of cognitive function which cannot be attributed to major psychiatric disorder [Albert et al., 2011; McKhann et al., 2011]. Dementia is believed to be caused in more than two thirds of the cases by Alzheimer's disease (AD), Vascular dementia (VaD) or a combination of both according to the Swedish Dementia Registry (SveDem). The clinical diagnosis is based on clinical presentation, neuropsychological and language therapist testing, neuroimaging findings and/or cerebrospinal fluid (CSF) examination.

Alzheimer's disease is the most common type of dementia and accounts for 31% of the cases [Religa et al., 2015]. AD typically begins with subtle cognitive problems, mostly in the memory domain, which slowly develop, become more severe and finally impair daily life. The continuum of AD development has been divided into three phases: (1) pre-clinical, (2) prodromal and (3) dementia. The pre-clinical stage of AD includes cognitively normal subjects who have AD pathologies. They may never experience clinical symptoms but the hypothetical assumption is that should the subjects live long enough they ultimately become symptomatic AD. Prodromal AD is the next stage when individuals experience subtle cognitive declines, subjective or appreciable with neuropsychological tests, but not to the extent that impacts daily functioning [Bäckman et al., 2005]. Dementia is the final stage when the cognitive impairment becomes severe enough to interfere with the patient's daily activities.

Vascular dementia is the second most common type of dementia and accounts for 18% of the dementia cases [Religa et al., 2015]. It usually emerges from continuous vascular damages such as small vessel disease (SVD) or sudden damages such as stroke. As opposed to AD, VaD usually begins with impairment in non-memory cognitive functions and memory impairment develops at later stages.

Pathological evidences show the pathologies of more than one type of dementia can be simultaneously evident in the brain. In those cases, the individual is considered to have mixed dementia. Mixed dementia is diagnosed when symptoms and biomarkers associated with more than one dementia, most commonly AD and VaD, are observed. Although mixed dementia accounts for just 18% of the dementia cases [Religa et al., 2015], it is estimated that mixed dementia is much more common than what was previously believed [Kovacs et al., 2013; White et al., 2005].

Since the definite diagnosis can be confirmed only *post-mortem*, biomarkers are a crucial part of both research and clinical practice. Biomarkers are variables (physiological, biochemical, anatomical) that can be measured *in-vivo* and that indicate specific features of disease-related pathological changes [Strimbu and Tavel, 2010]. There are three major groups of biomarkers for differential diagnosis of individuals with cognitive impairment that monitor different aspects of brain changes:

- ***Brain Amyloid beta (Aβ) deposition***
    - Positive positron emmision topography (PET) amyloid imaging on e.g. Pittsburgh compound B (PiB) PET
    - Decrease in Aβ42 levels in CSF examination
- ***Neuronal degeneration or injury***
    - Increase in total and/or phosphorylated tau protein in CSF examination
    - Cerebral hypometabolism on ^{18}Fludeoxyglucose (FDG) PET
    - Morphological changes
        - Hippocampal atrophy on magnetic resonance imaging (MRI) or computerized topography (CT)
        - Global cortical atrophy on MRI or CT
        - Cortical thining visible on MRI
    - Cerebral hypoperfusion on single photon emission computerized topography (SPECT)
- ***Cerebrovascular damages***
    - T2 and fluid-attenuated inversion recovery (FLAIR) for white matter hyperintensities (WMH)
    - T2* and susceptibility weighted images for detecting cerebral microbleeds
    - Diffusion tensor imaging (DTI) for measuring white matter integrity

These biomarkers do not become abnormal and detectable simultaneously but do follow a specific temporal pattern. The generally accepted hypothesis is that they follow an S-shape curve and their detectability thresholds come in a roughly specific order. For example, in AD, which is the most prevalent cause of cognitive impairment and dementia, the first change is Aβ deposition detectable through PET amyloid imaging and CSF Aβ42 examination. The next change is the increase of tau protein in CSF which is an indicator of neuronal injury. The change in brain morphology, metabolism and perfusion comes next, at approximately the same time, followed by cognitive impairment symptoms. [Jack et al., 2013, 2010]

1.2 NEUROIMAGING IN COGNITIVE IMPAIRMENT

Neuroimaging is an integral part in the process of diagnosing different causes of cognitive decline as well as an essential tool in research. In Sweden, 94% of patients undergo neuroimaging examination during their basic dementia workup [Falahati et al., 2015]. It is a crucial step as it can monitor biomarkers for the diagnosis of individuals with dementia *in-vivo* which among others includes medial temporal lobe atrophy (MTA) visible in MRI, reduced glucose metabolism visible on FDG-PET and Aβ deposition detectable with PiB-PET. However, there is no single test for the diagnosis and neuroimaging serves as a complementary diagnostic and research tool.

Many imaging modalities have been used in the clinical workup and research settings to measure different aspects of disease pathologies. Although MRI is the preferable tool for assessing morphological changes, CT is still the most used modality in clinical routine. Due to the significantly higher cost of PET and availability of CSF examination in Sweden, PET is only used in a limited number of cases in the specialized units (Table 1). Figure 2 illustrates typical changes in cognitively impaired brains visualized using different modalities.

The focal point of this thesis is the interaction between the changes in white matter (WM) and gray matter (GM) in individuals with early signs of cognitive impairment. Those changes are best visualized and measured using MRI scans, namely T1 scans for GM changes, and fluid-attenuated inversion recovery (FLAIR) and diffusion tensor imaging (DTI) for measuring changes in the WM.

Gray matter changes in the form of cortical thinning and atrophy are associated with the emergence and progression of neuronal loss. GM changes are well studied and constitute the most used neuroimaging biomarker in clinical routine. For example, the atrophy in the temporal lobe and in particular hippocampus and entorhinal cortex are the signature of AD dementia.

Damage to the WM has also been reported to contribute to the development of cognitive impairment. Most evidence comes from epidemiological studies and suggests a higher burden of WMH associates with higher incidence of dementia [Buyck et al., 2009; Coffey et al., 1989; Debette et al., 2010; Prins et al., 2005], more cognitive decline [Vermeer et al., 2003], higher levels of Aβ deposition [Gurol et al., 2006; Marchant et al., 2012] and reduced functional connectivity [Zhou et al., 2015]. Some studies have considered more
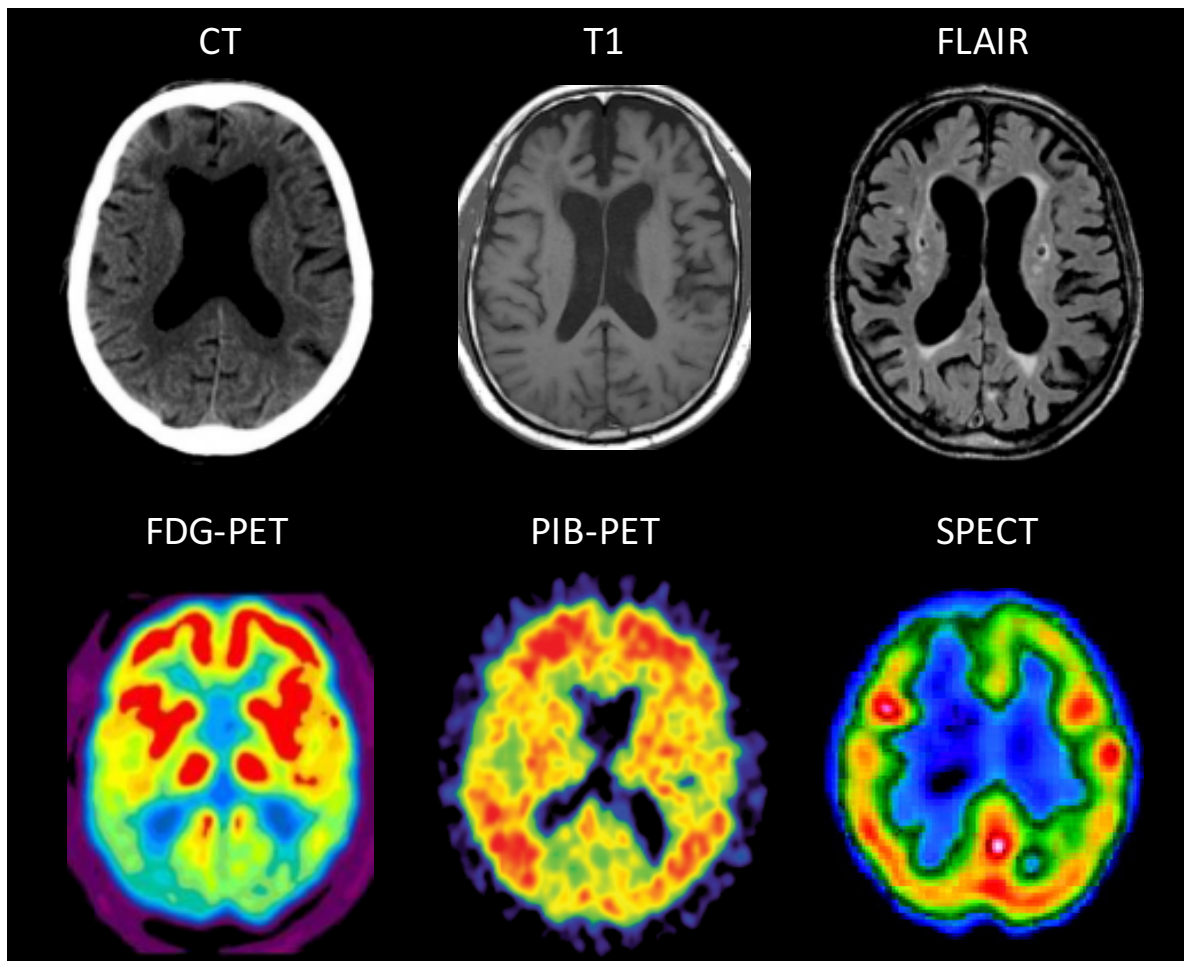
Figure 2 Example of different neuroimaging modalities commonly used in dementia research and clinical use.

Modality	AD related finding	Availability	Usage
CT	Crude morphological changes	Highly available	87%
MRI		Highly available	16%
Structural	GM atrophy, lesions		
Functional	Abnormal functional connectivity		
DTI	Loss of white matter integrity		
Nuclear Imaging		Specialized units	6%
FDG-PET	Hypometabolism in temporal lobe		
Amyloid-PET	Amyloid deposition		
SPECT	Hypoperfusion in temporal lobe		

Table 1 Imaging modalities used in dementia care. Data from SveDem http://www.ucr.uu.se/svedem/.

	FA	MD	DA	RD
Normal WM	High	–	High	Low
High myelination WM	High	Low	–	Low
Axonal injury	Low	High	Low	High
Demyelination	Low	High	–	High

Table 2 Change in diffusion parameters of white matter. WM: white matter. FA: fractional anisotropy. DA: axial diffusivity. RD: radial diffusivity.

detailed measures of WMH and showed similar results when measuring WMH in different spatial location [Holland et al., 2008; Taylor et al., 2017; Tullberg et al., 2004].

1.3 WHITE MATTER CHANGES IN COGNITIVE IMPAIRMENT

Traditionally, AD has been assumed to be a disease of the GM and the damage in WM was considered secondary to the GM damage. Advances in neuroimaging techniques have contributed to further understanding of the role of WM damages in cognitive impairment.

Neuroimaging techniques that detect WM damage infer the damage through measurement of the water diffusion or water content. Water diffusion can be imaged with diffusion tensor imaging (DTI). One can obtain information about the underlying properties of WM by studying the diffusion properties. Fractional anisotropy (FA), mean diffusivity (MD), axial diffusivity (abbreviated here as DA to avoid confusion with the abbreviation used for Alzheimer's disease) and radial diffusivity (RD) are the most common diffusion measures. The concrete relationship between diffusion measures and neurobiology of WM is not completely known. However, an increase in the diffusivity perpendicular to the perceived direction of WM fibers may reflect demyelination as the loosening of myelin sheaths allows for less restricted diffusion perpendicular to the axons. Similarly, a decrease in the diffusivity parallel to the perceived direction of WM fibers may indicate axonal injury (Table 2).

Another use of DTI, or rather of diffusion weighted imaging in general, is tractography. Tractography is a modeling method in order to represent WM tracts by connecting the perceived directions of WM tracts, derived from the directional distribution of water diffusion.
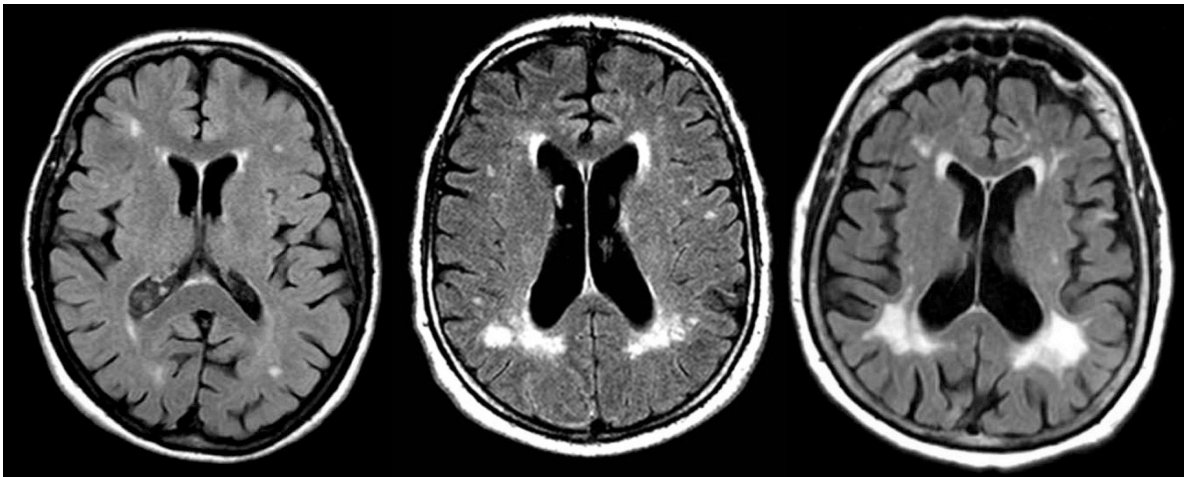
Figure 3 Different burden of white matter hyperintensities showed on FLAIR images.

Water content of the WM can be measured using traditional MRI techniques. Normal WM which has structured axons has a high lipid content. Therefore, normal WM appears hyperintense on T1-weighted images and hypointense on T2-weighted images. On the other hand, if, due to different pathological process (e.g. inflammation, ischemia or demyelination), WM becomes less hydrophobic with higher water content, it becomes hypointense on T1-weighted MRI images and hyperintense on T2-weighted images. The areas that appear as hyperintensities on T2-weighted and FLAIR images are called white matter hyperintensities (WMH) (Figure 3). They are radiological findings and look similar independent of the underlining pathological process.

White matter hyperintensities correspond to tissue damage (ischemia/infarction, gliosis, rarefaction, loss of myelin, microglial infiltration, inflammation, and amyloid angiopathy) that is likely to cause disconnection of functionally-related cortical and subcortical structures that are important to cognitive function and speed. WMH are common especially for patients with different degrees of cognitive impairment: AD, VaD and mild cognitive impairment (MCI). Although WMH are very common pathological processes, their role in the abovementioned conditions is still far from being understood.

Epidemiological studies have shown that WMH are often already present at a young age and their prevalence increases with age. Forty two percent of young adults, 80% of 55-65 year olds and 92% of people aged 65 and older have detectable WMH and 19.5% of older adults aged 65 and older have severe WMH [Garde et al., 2000; Liao et al., 1997; Ylikoski et al., 1995]. WMH are more prevalent in patients with cardiovascular risk factors. Hypertension [Havlik et al., 2002; Schmidt et al., 2003; van Dijk et al., 2004], coronary heart disease, diabetes and atherosclerosis [Manolio et al., 1999] are among the most important risk factors for developing WMH.

1.4 MEASUREMENT OF WHITE MATTER CHANGES

Visual assessment is the fastest and easiest way of measuring WMH burden. Visual assessment of WMH in the clinical settings is performed using Fazekas scale [Fazekas et al., 1987]. The Fazekas scale is a four-level scale that quantifies the overall presence of WMH in the entire brain. It is best scored on FLAIR or T2-weighted images as:

- Fazekas 0: None or a single punctate WMH
- Fazekas 1: Multiple punctate WMH
- Fazekas 2: Beginning confluency of WMH (bridging)
- Fazekas 3: Large confluent WMH

In addition, in research settings several other visual rating scales are employed [Scheltens et al., 1998, 1993; Wahlund et al., 2001] all of which provide an impression of the burden of WMH in different brain regions. Visual scales are a fast and easy method, and they do correlate with clinical outcomes [Pantoni et al., 2002]. However, visual scales have low variability, cannot be incorporated in automated imaging pipelines and thus may not provide enough information for in-depth investigations. On the other hand, computerized segmentation of WMH can provide detailed quantification of the WMH burden and can be used in automated imaging pipelines. However, the usability of computerized methods is still limited. First, they usually require specific technical equipment, and second, they are challenging to use in large or multicenter studies or clinical trials. Employing computerized methods is precarious since they are sensitive to resolution, image contrast and acquisition parameters and settings, and to some degree, even to the burden of WMH. Most computerized measurements are not reproducible and require human interaction at some point. Currently, due to these technical hurdles, the measurement of WMH is not reliable enough and may even lead to inconsistent correlations with clinical variables [Gouw et al., 2008; van Straaten et al., 2006]. Therefore, an accurate way of measuring WMH is very much required.

Computerized methods generally consist of pre-processing, core segmentation and post-processing steps. Methods are classified based on the core-segmentation as supervised [Steenwijk et al., 2013; Zijdenbos et al., 2002], unsupervised [Raniga et al., 2011; Schmidt et al., 2012; Shiee et al., 2010] or based on mathematical definition of WMH [Zhu and Basir, 2003]. As a result of recent improvements in machine learning techniques, such core methods are now able to produce decent classifications once given properly prepared data. However, feature selection and pre-processing are not robust enough to make a method

reproducible under different condition. We believe that, in order for a method to be reproducible in all conditions at least one of the following conditions must be satisfied:

- Pre-processing normalizing the input image to a defined resolution, intensity range, and defined search area independent of imaging sequence or WMH burden.
- Feature selection rendering the intensities of the image to features independent of imaging sequence or WMH burden.
- Core-segmentation method classifying the images independent of imaging sequence or WMH burden.

Usually methods address all of the above-mentioned points to some extent, however to date no method has been presented that fully handles one or many of them.

Another difficulty in assessing WM is related to diffusion imaging. While DTI metrics such as FA or MD can be quantified, tractography in the presence of WMH is next to impossible. In a nutshell, tractography estimates the direction of WM tracts at each point and reconstructs the tract path by subsequently connecting the estimated tract directions. In areas with severe WM damage, such as WMH, reliable estimation of the tract direction may not be possible and thus traditional tractography can fail in the presence of WMH or other WM damage.

These technical difficulties contribute to the fact that in many studies subjects with a high burden of WMH are excluded. As a result, little evidence is available to support or reject the role of WM damage in AD or other dementias in contrast to the established consensus about the role of GM atrophy. In the first part of this thesis, technical difficulties in processing subjects with a high burden of WMH were addressed and methods developed for WMH measurement. In the second part, the methods created in the first part, have been used to investigate the role of WMH and GM atrophy in the earliest stages of the development of cognitive impairment.

2 AIMS

The main aims of this thesis are:

   I.   To develop and validate an automated tool for the segmentation of WMH using different MRI sequences

  II.   To study the role of cerebrovascular risk factors on WMH and brain structural changes

 III.   To study the interaction between WMH, brain structures and cognition in cognitively healthy controls (CTL) , subjective cognitive impairment (SCI) and MCI subjects

In particular, the aims of the thesis are achieved through the following studies:

Study I: To develop an automated tool for segmentation of WMH

Study II: To validate the automated tool developed in ***Study I***, in different research scenarios to ensure its usability for answering our medical research questions independent of imaging sequence and WMH burden

Study III: To study the long-term effect of coronary heart disease (CHD) on WMH and brain structural change

Study IV: To investigate the relationship between GM atrophy and WMH in anatomically connected WM tracts in CTL, SCI and MCI subjects.

3 MATERIALS AND METHODS

3.1 ETHICAL CONSIDERATION

For all the studies, we have used pre-acquired data from Norway, England, Finland and Sweden. All ethical permissions have been acquired from the authorities in respective countries. Ethical permission for *Study IV* for which data was acquired in Sweden corresponds to document number 2008-695 and 2010-156. All procedures performed in the studies were in accordance with the ethical standards of the institutional and national research committees and with the 1964 Helsinki declaration and its later amendments or comparable ethical standards.

3.2 SUBJECTS

3.2.1 Study I: DemWest cohort

Data from the Dementia Study in Western Norway (DemWest) from three centers in western Norway has been used. The study employs MRI scans of 102 subjects including CTL, AD, Lewy body dementia (LBD) and Parkinson disease dementia (PDD). Diagnosis was made according to consensus criteria for AD, LBD and PDD using standardized clinical instruments, blood tests and MRI. Details of the selection and diagnostic procedures are reported elsewhere [Aarsland et al., 2008]. The imaging protocol included: sagittal 3D T1-weighted and 2D FLAIR. All images had been acquired with a 1.5 Tesla scanner and had full brain and skull coverage.

	ST(mm)	SG(mm)	TE(ms)	TR(ms)	TI(ms)	AF(deg)
3D T1 Stavanger	2	-	4.6	10.0	-	30
2D FLAIR Stavanger	4	1	100	6000	2000	90
3D T1 Haugesund	1	-	4.6	20.0	-	30
2D FLAIR Haugesund	4	1	110	6000	2000	90
3D T1 Bergen	1	-	3.1	8.2	500	7
2D FLAIR Bergen	4	1	105	7927	1981	90

Table 3 MRI parameters for the DemWest cohort. ST: Slice thickness, SG: Slice gap, TE: Echo time, TR: Repetition time, TI: Inversion time, AF: Flip angle.

	ST(mm)	SG(mm)	TE(ms)	TR(ms)	TI(ms)	AF(deg)
3D T1	1.2	-	3.80	8.6	1000	8
2D PD	3	3	10.58	3000	-	90
2D T2	4	5.5	88.16	5000	-	90
2D FLAIR	4	5.5	160.70	10000	2500	90

Table 4 MRI parameters for the KHP-DCR cohort. ST: Slice thickness, SG: Slice gap, TE: Echo time, TR: Repetition time, TI: Inversion time, AF: Flip angle.

3.2.2 Study II: KHP-DCR cohort

Data from King's Health Partners-Dementia Case Register (KHP-DCR) in the UK was used for this study. MRI scans of 119 subjects (AD, MCI, CTL) were used. The AD diagnosis was made according to the Diagnostic and Statistical Manual for Mental Diagnosis IV (DSM-IV) [American Psychiatric Association, 1994] and MCI was defined according to the Petersen criteria [Petersen et al., 1999]. The imaging protocol included: sagittal 3D T1-weighted, axial proton density (PD), T2-weighted fast spin echo image, and 2D FLAIR. All images had been acquired with a 1.5 Tesla scanner and had full brain and skull coverage and quality control was performed according to the AddNeuroMed image quality protocol [Simmons et al., 2011].

3.2.3 Study III: CAIDE cohort

Data from the Cardiovascular Risk Factors, Aging and Dementia (CAIDE) study, performed in Eastern Finland, was used. CAIDE is a longitudinal, population-based study to assess the association between cardiovascular and life-style risk factors, and cognitive impairment and dementia. Participants were first evaluated between 1972 and 1987 in a study to evaluate the risks, morbidity and mortality of cardiovascular diseases. The first re-examination was performed in 1997 on a random sample of 2000 participants. The second re-examination was conducted between 2005 and 2008. Cognitive status was assessed in both re-examinations with a three-step protocol: (1) screening, (2) clinical and (3) differential diagnosis, which includes brain MRI. One hundred and thirteen subjects that participated in the differential diagnosis in the second re-examination had MRI. For this study, subjects with dementia diagnosis and subjects with very low MRI quality were excluded and in total 63 MCI subjects and 6 CTL subjects were used. Table 5 shows the MRI parameters for the subjects used in this study.

14

	ST(mm)	SG(mm)	TE(ms)	TR(ms)	TI(ms)	AF(deg)
3D T1 Magnetom Vision	1.5-2.0	-	4.0	9.7	300	12
3D T1 Avanto	1.0-1.5	-	3.93	1900	1100	15
2D FLAIR	5	5	119	9000	2200	180

Table 5 MRI parameters for the CAIDE cohort. ST: Slice thickness, SG: Slice gap, TE: Echo time, TR: Repetition time, TI: Inversion time, AF: Flip angle.

3.2.4 Study IV: BioFINDER I cohort

Data for this study was from part of the Swedish Biomarkers for Identifying Neurodegenerative Disorders Early and Reliably (BioFINDER) study. In this study two cohorts from the BioFINDER were used: (1) Cognitively healthy elderly and (2) Patients with mild cognitive symptoms including SCI and MCI.

People without any cognitive symptoms, older than 60 years of age, Mini-Mental State Examination (MMSE) greater than 28 at screening that do not fulfill the criteria for MCI or any dementia were recruited as CTL group. People with mild cognitive symptoms were recruited from those referred to the memory clinics due to cognitive symptoms experienced by the patient or informant, age between 60 and 80 years, MMSE greater than 24 that does not fulfill criteria for any dementia. Individuals with no significant impairment in any further test were grouped as SCI and the rest as MCI. Exclusion criteria for all groups were significant unstable systemic illness or organ failure, such as terminal cancer, current significant alcohol or substance misuse or cognitive impairment that can be explained by another condition or disease such as normal pressure hydrocephalus, major cerebral hemorrhage, brain infection, brain tumor, multiple sclerosis, epilepsy, psychotic disorders, severe depression, alcohol abuse in the last five years and on-going consumption of drugs that regularly cause cognitive symptoms. The detailed description of the cohort as well as recruitment procedures and eligibility criteria is available at http://BioFINDER.se.

Four hundred and sixty-eight subjects with available MRI images (T1, FLAIR, DTI) with parameters presented in Table 6 are used for this study. MMSE and A Quick Test of Cognitive Speed (AQT) were used to assess the cognitive performance.

	ST(mm)	SG(mm)	TE(ms)	TR(ms)	TI(ms)	AF(deg)
3D T1	1.2	-	3.37	1950	900	9
3D FLAIR	4.0	-	89	9000	2500	130
2D DTI	2.0	2.0	86	8200	-	90

Table 6 MRI parameters for the BioFINDER cohort. ST: Slice thickness, SG: Slice gap, TE: Echo time, TR: Repetition time, TI: Inversion time, AF: Flip angle.

3.3 IMAGE PROCESSING

3.3.1 Study I and II

The first two studies aimed at developing and validating a fully automated WMH measurement tool. In ***Study I***, a fully automated supervised WMH segmentation method was developed using a cascade of support vector machines (SVM), hence the software name Cascade.

Study II aimed to validate and make the previously developed WMH segmentation tool unsupervised and completely independently of manual interaction or segmentation. The improved WMH segmentation method took advantage of the initial method in its calculation of evident normal brain (3.3.1.2 below). The final WMH measurement algorithm, published as paper II, consists of four main steps:

  I.   Pre-processing
  II. Calculating the evidently normal brain
  III. White matter hyperintensities definition
  IV. Correction for multiple comparison and reporting

3.3.1.1   Pre-processing

The aim of the pre-processing was to register all input sequences together, correct them for inhomogeneity and estimate initial brain tissue segmentation as WM, GM and CSF. Pre-processing comprised the following steps:

  I.   Intra-subject registration using 3D rigid transformation with mutual information as the similarity measure using FSL FLIRT [Jenkinson and Smith, 2001].
  II. Brain extraction using FSL BET [Smith, 2002].
  III. Inhomogeneity correction for all registered input images using the N3 algorithm [Sled et al., 1998].
  IV. Brain tissue segmentation into GM, WM, and CSF using FSL FAST [Zhang et al., 2001].

V.   Refining brain tissue segmentation: GM-labeled voxels that were bright on either FLAIR or T2 images (top 15% voxels of GM intensity histogram) and surrounded by mostly WM were re-labeled as WM

3.3.1.2   Calculating evident normal brain

The proposed definition of WMH (3.3.1.3 below) requires a WMH free area as a reference. The aim of calculating evident normal brain was to have such an area with almost no WMH in it. In the studies, we used the following two simple steps:

I.   Capture the hypointense area of FLAIR (45%), T2 (50%), and/or PD (65%) and the hyper-intense area of T1 (15%) with thresholding. The thresholding was performed in 1 mm, 2 mm, and 3 mm spatial scales (Figure 4-A).

II.   Thresholding using an optimal threshold calculated to resemble the mask calculated in the first step. The threshold was calculated using a single node SVM reduction algorithm [Schölkopf et al., 1999].

A *proper closing* morphological filter was then applied to the mask captured with both above steps (AND operation) in order to fill small holes. *Proper closing* is defined using morphological closing (C), and opening (O) functions with two-millimeter spherical structuring element.

$$Proper\ Closing(M) \stackrel{\text{def}}{=} M \wedge O\left(C\left(O(M)\right)\right)$$

The output voxels of the morphological filtering were considered as an evident normal brain (Figure 4-B).
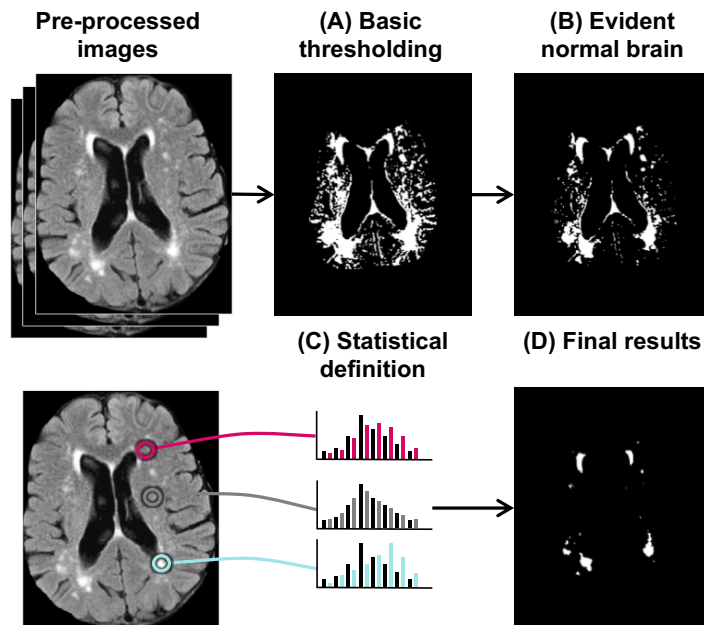

Figure 4 Steps in segmentation of white matter hyperintensities using statistical definition.

3.3.1.3 White matter hyperintensities definition

We reformulated the common definition of WMH which is based on the appearance of the area on each image (hyperintensities or hypointensities) into a statistical definition that can be calculated robustly:

White matter hyperintensities are areas in the WM in which their local image histograms are significantly different from the local histogram of the evidently normal brain on the one-tailed statistical test.

This statistical definition can be applied to T1, T2, FLAIR and PD sequences (Figure 5) and is explicitly and implicitly independent of manual delineation. In the studies included in this thesis, a one-tailed Kolmogorov–Smirnov test (significance level 0.05) was used to test the significance of WMH definition.
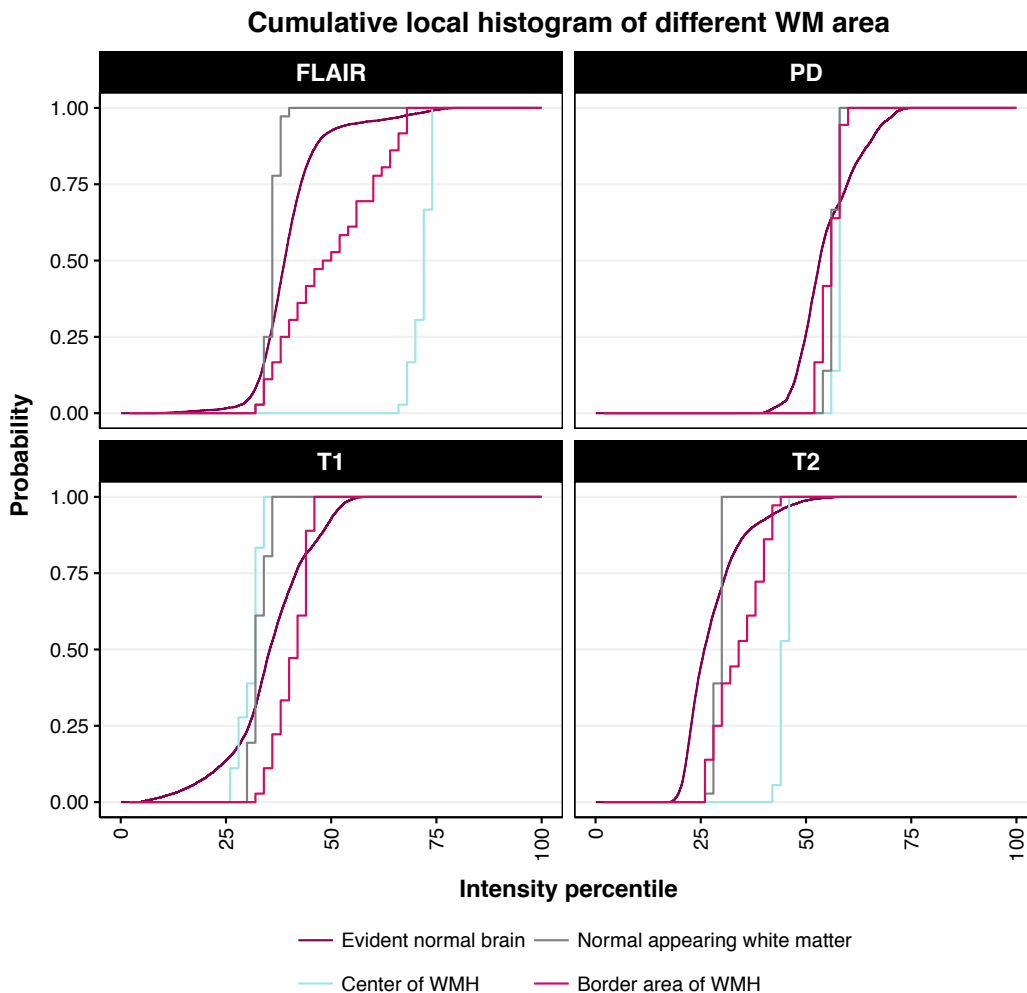

Figure 5 Local image histogram of T1, T2, FLAIR and PD sequences compared with the local histogram of evident normal brain.

3.3.1.4 Correction for multiple comparison and reporting

The WMH definition assigns a p-value to each voxel. Since there are millions of voxels to be tested, one needs to correct the possibility of false discovery due to presence of multiple tests. To deal with this problem, the p-value map was first converted to a binary map and all segments which do not contain a fully connected (26-connected) patch of voxels were discarded. Finally, the significant segments were considered to be the WMH mask. Post processing then removed all detection that was connected to the cortex or that was smaller than 27mm^3 to create the final segmentation Figure 4-D.

3.3.2 Study III

The image processing in this study consist of analyzing gray matter and white matter:

 I.   Cortical thickness and brain tissue volume extracted using the CIVET pipeline available through the McConnell Brain Imaging Centre, Montreal Neurological Institute, McGill University, Montreal, Canada (http://www.bic.mni.mcgill.ca/).
 II. Measurement of the WMH volume using Cascade (***Study I*** and ***Study II***).

Firstly, cortical thickness and brain tissue volume were calculated using the CIVET pipeline (Appendix I). The outputs extracted from the CIVET pipeline were cortical thickness maps, total WM volume and total GM volume. Cortical thickness maps were further analyzed using an in-house MATLAB script to assess difference in cortical thickness in different groups, to visualize and to prepare the data for further use in the statistical analysis. Secondly, Cascade was used to calculate the WMH volume using T1 and FLAIR images.

3.3.3 Study IV

The image processing in this study consisted of several parts:

 I.   GM parcellation using FreeSurfer software suite recon-all command (Appendix I).
 II.   WMH segmentation using Cascade (***Study I*** and ***Study II***).
 III. Measurement of the WMH burden in tracts connected to each GM region.

A software program was developed for the third step. The software isolates the WM tracts connecting each GM region to the rest of the brain and measures the amount of WMH on each connecting tract, henceforth *tract-based WMH* (Figure 6). The software, called Connectivity (https://github.com/Damangir/Connectivity), includes the following steps:

I. DTI pre-processing and parameter estimation
II. Tractography on WMH free subjects to generate a database specific atlas of tracts
III. DTI atlas propagation
IV. *Tract-based WMH* measurement

3.3.3.1 *DTI pre-processing and parameter estimation*

Firstly, DTI images were corrected for eddy current distortions and head movement; then diffusion tensors were fitted to calculate fractional anisotropy (FA), mean (MD), axial (DA), and radial diffusivity (RD). These values were needed for the rest of the processing.

3.3.3.2 *Tractography on WMH-free subjects to generate a database specific atlas of tracts*

DTI images were used to calculate the probabilistic atlas of tracts connecting GM areas to the rest of the brain. This procedure was only performed on images with low WMH burden (Fazekas scale 0 and 1). The following procedure was performed in order to create the connectivity atlas:

I. Estimation of the diffusion parameters per voxel using a two-fiber model using FSL bedpostx [Behrens et al., 2003].
II. Calculating the WM tracts connected to all previously segmented GM regions using FSL probtrackx2 [Behrens et al., 2003]. Each 72 GM region was separately set as a seed region with brain boundaries as the stopping criteria and 5000 streamline per voxel.
III. Nonlinearly registering the calculated tracts to MNI space and then averaging them to obtain probabilistic distributions of tracts for each region using FSL FNIRT.

The average tract distribution formed the database specific atlas of connectivity and was used in the rest of the analysis.

3.3.3.3 *DTI atlas propagation*

In order to measure the WMH on each tract, the probabilistic atlas of connectivity needed to be in the subject's native space. This procedure is performed on all subjects including those with low WMH used in the previous step:

I. Calculating the nonlinear transformation between the MNI space (connectivity atlas) and each subject's native space using FA images and masking the area with WMH.
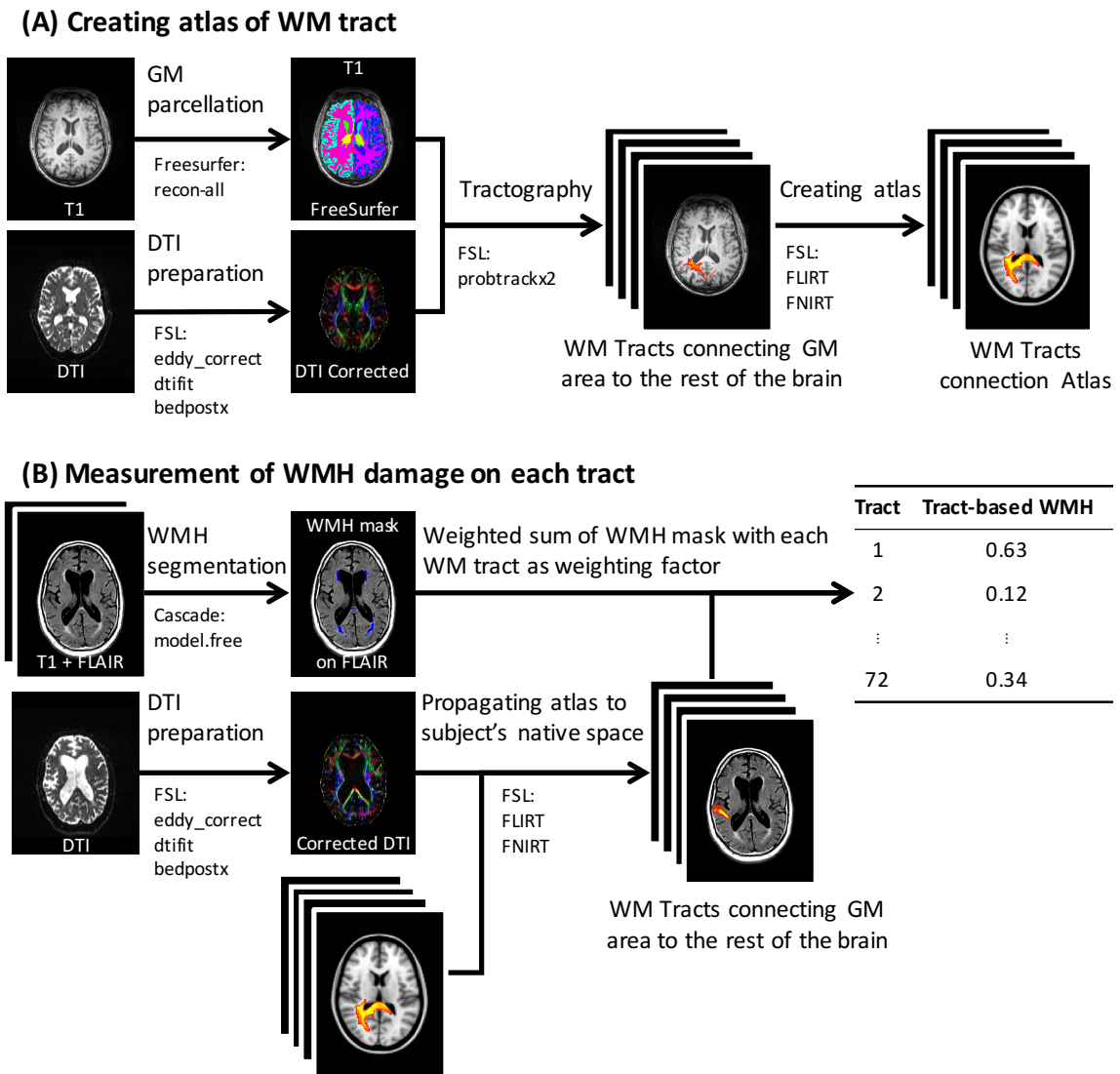II. Registering the probabilistic connectivity atlas to subject's native space using the calculated transformation.

20

(A) Creating atlas of WM tract

(B) Measurement of WMH damage on each tract

Tract	Tract-based WMH
1	0.63
2	0.12
⋮	⋮
72	0.34

Figure 6 Connectivity pipeline for quantification of the tract-based white matter hyperintensities.

3.3.3.4   Tract-based WMH *measurements*

Once the probabilistic connectivity atlas is registered to the native space, *tract-based WMH* can be calculated as the weighted sum of the WMH map with each tract of the probabilistic connectivity map as the weighting factor. Figure 6 presents the full pipeline for measurement of *tract-based WMH*.

3.4   STATISTICAL ANALYSIS

Study I: A receiver operating characteristic (ROC) curve was used to assess the effectiveness of the algorithm. Pearson correlation was used to compare the segmented volume and manual delineated volume of WMH. All the analysis and visualization were performed in MATLAB 7.12 (The MathWorks Inc., Natick MA, USA, 2011).

Study II: Pearson correlation was used to compare the calculated WMH volumes and manual delineated WMH volumes. In order to assess the classification quality and compare the automatic segmentation to manual delineation, false negative rate, false discovery rate and the Dice coefficient [Dice, 1945] were used. MATLAB 8.4 (The MathWorks Inc., Natick MA, USA, 2014) was used for statistical analysis and visualization.

Study III: Group-wise comparison of the cortical thickness in the whole brain and its corresponding visualization was performed using MATLAB 7.6 (The MathWorks Inc., Natick MA, USA, 2008). T-test was used to compare the two groups and false discovery rate (FDR) was used to correct for multiple comparisons. IBM SPSS Statistics for Windows 19.0 (IBM Corp., Armonk, NY, USA, 2010) was used for all other statistical analysis and visualization. To explore the population characteristics, t-test and chi-squared were used for continuous and categorical variables respectively. Linear regression was used to investigate the possible effect of CHD and blood pressure on the regional cortical thickness, WMH volume and GM volume. Where applicable the analyses were corrected for age, follow-up time as well as the scanner type.

Study IV: R 3.1.0 (R Core Team, 2016) was used for statistical analysis and visualization. Normality of distributions was tested using the Shapiro–Wilk test. Group differences were analyzed using analysis of variance (ANOVA). The relationships between *tract-based WMH* and GM volume were modeled using generalized linear model (GLM). Interaction terms were introduced to the model to account for the possible effect of the diagnosis on the relationship. "Fraction of variance explained" refers to R-squared values, calculated using the model prediction according to the method proposed by Magee [Magee, 1990]. Differences in effects and interactions terms (i.e. between diagnosis and effects) were directly calculated within the GLM. Differences in fraction of variance explained was estimated by bootstrapping.

Throughout the thesis, corrected p-values < 0.05 were considered to be statistically significant. Normally distributed data are presented as mean and standard deviation (SD) and non-normally distributed data as median and interquartile range (IQR).

4 RESULTS

4.1 STUDY I AND II

Study I investigated the feasibility of Cascade as a WMH segmentation method. *Study II* focused on the reproducibility of the method for large multicenter data and validation of the WMH measurements obtained from different image modalities.

In the first two studies, measurement of WMH was performed in both a supervised and an unsupervised way. In *Study I*, WMH were classified with high sensitivity (90.0%) and specificity (99.5%) of which 2.3% in sensitivity and 0.4% in specificity attributed to post processing. The WMH volume obtained with Cascade was significantly correlated ($p < 0.01$) with the volume obtained from manual delineation.

Study II used a dataset with available T1, T2, FLAIR and PD sequences that have a large variety of WMH burden (median 20.5 IQR 26.2 cc). Large variation in WMH volume made the validation more reliable, but visualization more challenging. Therefore, the Dice coefficient and volume ratio were used for the purpose of visualization to be invariant of the total WMH volume.

Measured volumes of WMH using combinations of available sequences that contain either T2 or FLAIR were within 3% of the manual delineation volume (Figure 7). Although the WMH volume was highly underestimated in the absence of T2 or FLAIR, the WMH volume obtained without T2 and FLAIR still significantly correlated with the manual volumes.

Dice coefficient, which measures overlap between two segmentations, was in the range of similarity expected from manual inter-rater agreement when either T2 or FLAIR was used. Segmentations which contained both T1 and FLAIR had higher agreement compared to manual inter-rater agreement (Figure 8).

Apart from similarity with the manual delineation, the segmentation using different combinations of sequences was also compared to one another to ensure that they are comparable. This validation is crucial in studies where the data is pooled from already acquired datasets with different image sequences. The Dice coefficients between all segmentation using either FLAIR or T2 were more than 80%, which exceeds manual inter-rater agreement (Figure 9).
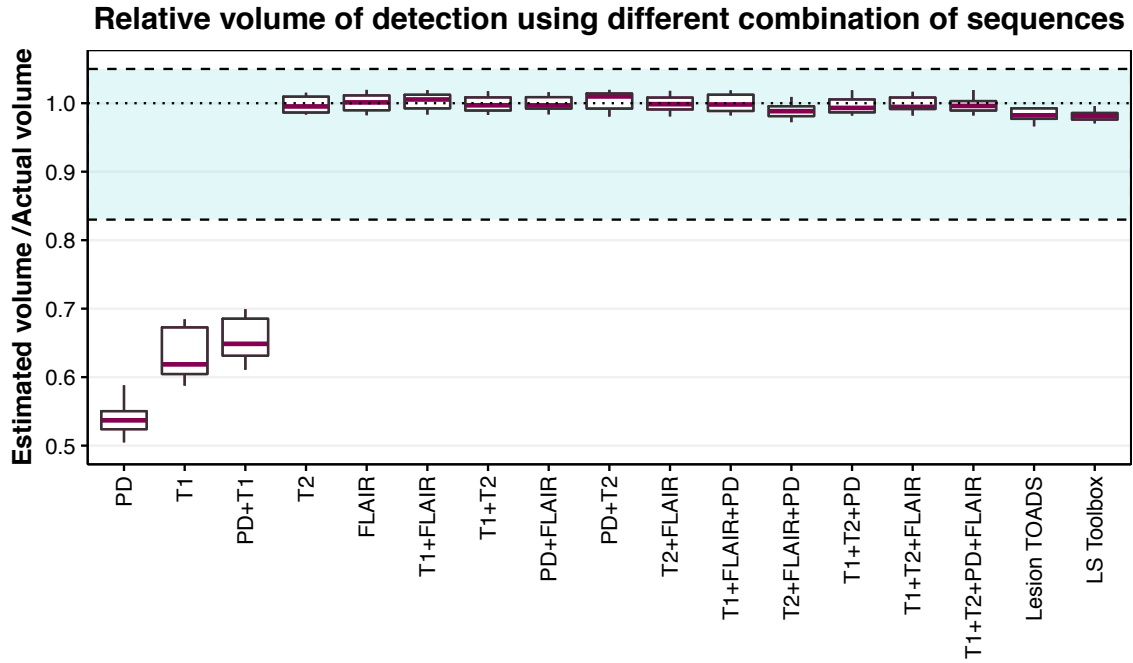
Figure 7 Ratio between segmented volume of white matter hyperintensities and volume from manual delineation.
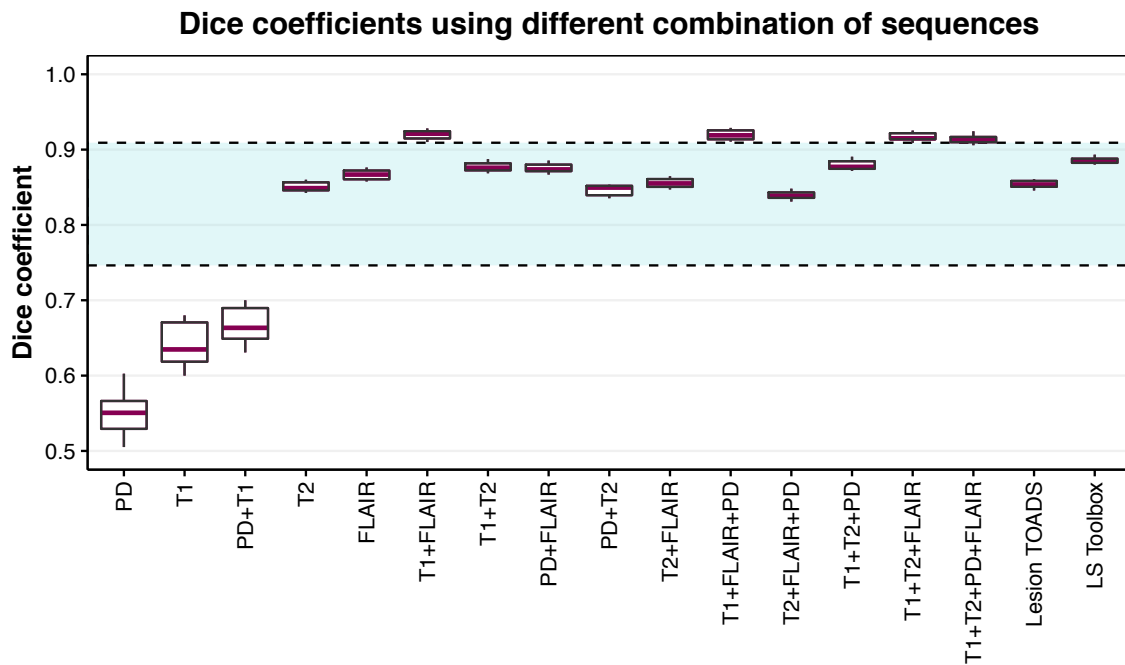

Figure 8 Dice coefficient between segmented white matter hyperintensities and manual delineation.

**Comparison between Dice coefficients
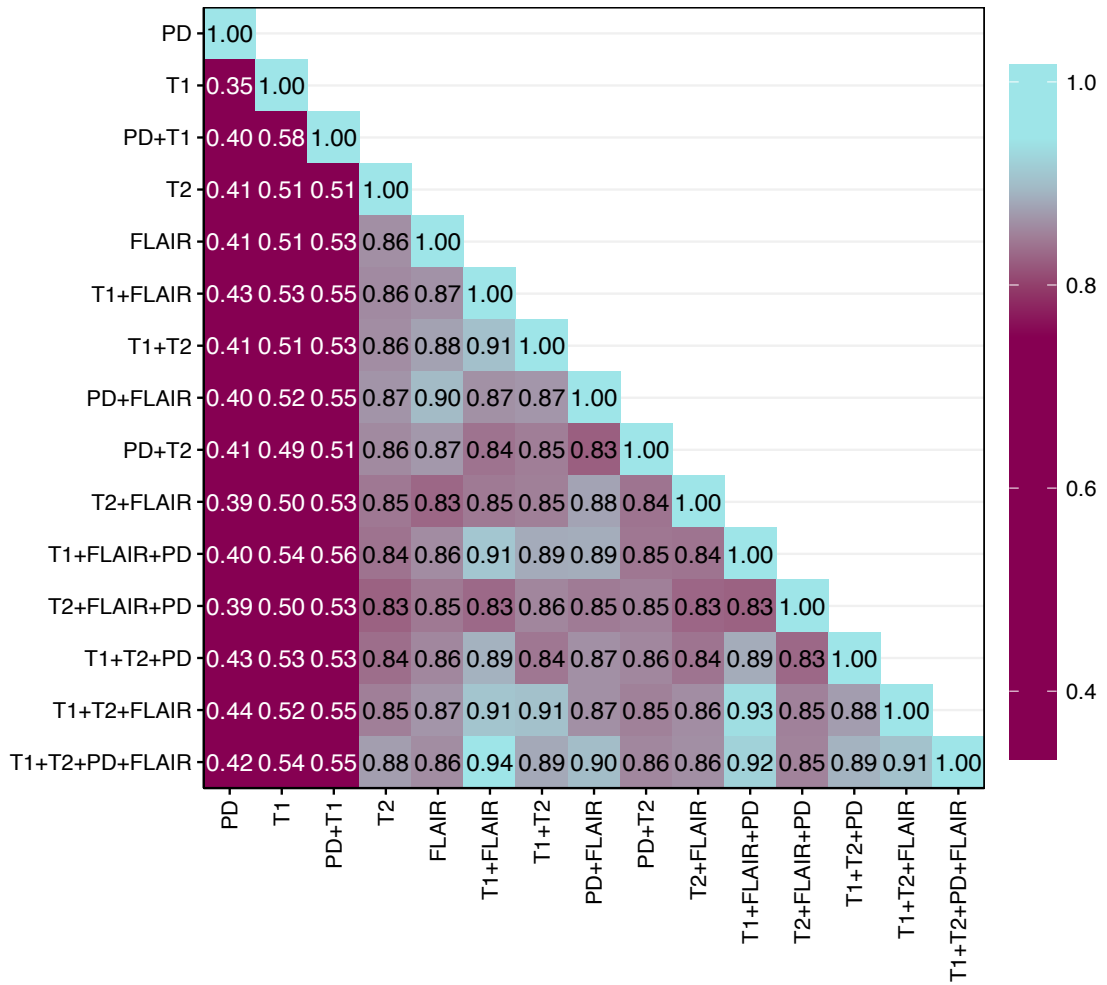using different combinations of sequences as reference**

	PD	T1	PD+T1	T2	FLAIR	T1+FLAIR	T1+T2	PD+FLAIR	PD+T2	T2+FLAIR	T1+FLAIR+PD	T2+FLAIR+PD	T1+T2+PD	T1+T2+FLAIR	T1+T2+PD+FLAIR
PD	1.00														
T1	0.35	1.00													
PD+T1	0.40	0.58	1.00												
T2	0.41	0.51	0.51	1.00											
FLAIR	0.41	0.51	0.53	0.86	1.00										
T1+FLAIR	0.43	0.53	0.55	0.86	0.87	1.00									
T1+T2	0.41	0.51	0.53	0.86	0.88	0.91	1.00								
PD+FLAIR	0.40	0.52	0.55	0.87	0.90	0.87	0.87	1.00							
PD+T2	0.41	0.49	0.51	0.86	0.87	0.84	0.85	0.83	1.00						
T2+FLAIR	0.39	0.50	0.53	0.85	0.83	0.85	0.85	0.88	0.84	1.00					
T1+FLAIR+PD	0.40	0.54	0.56	0.84	0.86	0.91	0.89	0.89	0.85	0.84	1.00				
T2+FLAIR+PD	0.39	0.50	0.53	0.83	0.85	0.83	0.86	0.85	0.85	0.83	0.83	1.00			
T1+T2+PD	0.43	0.53	0.53	0.84	0.86	0.89	0.84	0.87	0.86	0.84	0.89	0.83	1.00		
T1+T2+FLAIR	0.44	0.52	0.55	0.85	0.87	0.91	0.91	0.87	0.85	0.86	0.93	0.85	0.88	1.00	
T1+T2+PD+FLAIR	0.42	0.54	0.55	0.88	0.86	0.94	0.89	0.90	0.86	0.86	0.92	0.85	0.89	0.91	1.00

Figure 9 Dice coefficient between the segmented white matter hyperintensities using different sequences to one another.

4.2 STUDY III

Data from 69 individuals were analyzed. Of them, three patients were diagnosed with CHD at baseline, 19 at the first follow-up and 26 at the second follow up. Nineteen individuals diagnosed with CHD at the first follow-up were considered as the group with CHD and the remaining 50 individuals as the group without CHD. Demographic characteristics of both groups were not significantly different, but the group with CHD had lower SBP and DBP in the second follow-up (Table 7). The association of CHD and hypertension on subsequent change in the GM volume, WMH volume, and cortical thickness was analyzed using linear regression. The analyses were corrected for age, gender, follow-up time, and scanner type. Individuals with no CHD who had hypertension at midlife had the same association as the group with no CHD and no hypertension. Similarly, the participant with CHD who had no hypertension at midlife had the same association as the reference group except for the cortical thickness in the left anterior prefrontal cortex. In contrast, subjects with CHD who also had hypertension at midlife had stronger association between GM measures and CHD for many regions (Table 8). Interestingly, the associations for the WMH volume were not significantly different between all groups.

	All	No CHD	CHD	p
n	69	50	19	
Age (mean (SD))				
Midlife	49.87 (6.01)	49.19 (6.21)	51.66 (5.18)	0.13
First follow-up	70.51 (3.43)	70.37 (3.41)	70.89 (3.55)	0.58
Second follow-up	77.95 (3.49)	77.78 (3.46)	78.40 (3.63)	0.51
Gender = Female (%)	42 (60.8)	34 (68.0)	8 (42.1)	0.05
Education (mean (SD))	7.76 (2.59)	7.51 (2.46)	8.44 (2.90)	0.15
SBP (mean (SD))				
Midlife	148.86 (24.79)	146.72 (26.72)	154.47 (18.23)	0.25
First follow-up	158.61 (23.87)	162.79 (21.04)	147.37 (27.89)	**0.03**
Second follow-up	148.12 (21.54)	151.78 (22.31)	138.47 (16.22)	**0.02**
DBP (mean (SD))				
Midlife	90.55 (11.27)	89.50 (11.63)	93.32 (10.02)	0.21
First follow-up	85.15 (10.78)	86.60 (10.94)	81.25 (9.60)	0.09
Second follow-up	75.75 (11.20)	77.36 (10.98)	71.53 (10.95)	**0.05**
APOE careers	22 (38.6)	17 (40.5)	5 (33.3)	0.65

Table 7 Demographic information for the CAIDE cohort.

MRI measurements	No CHD Hypertension	CHD Hypertension	CHD No hypertension
n	16	10	9
Mean cortical thickness			
Left anterior insular cortex	0.01 (0.96)	**-0.54 (<0.01)**	-0.17 (0.15)
Right anterior insular cortex	-0.13 (0.21)	**-0.61 (<0.01)**	-0.14 (0.20)
Left angular gyrus	-0.13 (0.27)	**-0.50 (<0.01)**	-0.23 (0.05)
Right angular gyrus	0.04 (0.68)	**-0.47 (<0.01)**	-0.10 (0.35)
Left fusiform gyrus	0.02 (0.88)	**-0.52 (<0.01)**	-0.14 (0.23)
Right fusiform gyrus	-0.04 (0.70)	**-0.62 (<0.01)**	-0.20 (0.08)
Left anterior prefrontal cortex	-0.06 (0.62)	**-0.46 (<0.01)**	**-0.24 (0.04)**
Right anterior prefrontal cortex	-0.06 (0.59)	**-0.48 (<0.01)**	-0.12 (0.31)
Left superior parietal gyrus	0.05 (0.66)	**-0.42 (<0.01)**	-0.16 (0.19)
Left superior temporal gyrus	-0.05 (0.66)	**-0.52 (<0.01)**	-0.14 (0.24)
Right posterior middle frontal gyrus	-0.07 (0.52)	**-0.59 (<0.01)**	-0.06 (0.54)
Right orbitofrontal area	-0.03 (0.80)	**-0.58 (<0.01)**	-0.07 (0.54)
Right precentral gyrus	-0.03 (0.80)	**-0.52 (<0.01)**	-0.09 (0.42)
Right inferior frontal gyrus	-0.10 (0.34)	**-0.54 (<0.01)**	-0.07 (0.51)
Total GM volume	0.07 (0.29)	**-0.16 (0.01)**	-0.03 (0.64)
Total WMH volume	0.24 (0.07)	0.06 (0.63)	-0.02 (0.88)

Table 8 Neuroimaging measures of subjects with different cardiovascular diagnosis. Numbers presented as standardized coefficients (p-value). CHD indicate individuals with coronary heart disease diagnosed at the first follow-up and hypertension indicate individuals with SBP≥160 or DBP≥95 at baseline (midlife). All groups were compared against group with no CHD and no hypertension (n=34). Cortical measures were presented only for the area that has significant association in at least one group.

4.3 STUDY IV

Two hundred fifty-seven cognitively healthy, 87 SCI and 124 MCI subjects were studied. Table 9 presents the background information for different groups and Table 10 provides the overall description of the neuroimaging measure. CTL, SCI and MCI groups were significantly different in terms of age, gender and years of education, hence all analyses in this study were corrected for age, gender and years of education.

	CTL	SCI	MCI	p
n	257	87	124	
Age (mean (SD))	73.78 (5.09)	70.15 (5.72)	72.19 (5.69)	**<0.01**
Gender = Female (%)	157 (61.1)	49 (56.3)	55 (44.4)	**0.01**
Education (mean (SD))	12.27 (3.80)	12.82 (3.31)	11.27 (3.45)	**0.01**
Smoking (%)				**<0.01**
Never smoker	118 (45.9)	51 (60.7)	69 (62.2)	
Current smoking	20 (7.8)	4 (4.8)	12 (10.8)	
Former smoking	119 (46.3)	29 (34.5)	30 (27.0)	
MMSE (mean (SD))	29.02 (0.94)	28.39 (1.50)	27.11 (1.79)	**<0.01**
AQT test (mean (SD))				
Color	24.51 (4.38)	26.79 (6.37)	31.53 (9.04)	**<0.01**
Form	33.62 (6.42)	38.01 (10.61)	44.41 (14.89)	**<0.01**
Color and Form	66.10 (12.65)	76.93 (23.70)	87.95 (31.52)	**<0.01**

Table 9 Demographic information for the BioFINDER cohort.

	CTL	SCI	MCI	p
n	257	87	124	
GM volume (mean (SD))				
Temporal	2046.02 (215.92)	2053.82 (210.60)	2057.46 (230.02)	0.88
Frontal	2463.10 (273.18)	2470.30 (277.84)	2560.18 (302.09)	**0.01**
Parietal	3431.96 (389.65)	3476.32 (363.13)	3522.83 (405.28)	0.10
Occipital	2488.64 (291.50)	2540.62 (292.06)	2561.78 (296.95)	0.05
Hippocampus	7.27 (0.84)	7.23 (0.87)	6.70 (1.05)	**<0.01**
Tract-based WMH (mean (SD))				
Temporal	0.27 (0.02)	0.27 (0.02)	0.26 (0.02)	**<0.01**
Frontal	0.29 (0.02)	0.29 (0.02)	0.28 (0.03)	**<0.01**
Parietal	0.26 (0.02)	0.25 (0.02)	0.24 (0.02)	**<0.01**
Occipital	0.21 (0.02)	0.21 (0.02)	0.20 (0.02)	**<0.01**
WMH volume (mean (SD))	11.75 (15.16)	13.57 (16.69)	26.06 (29.05)	**<0.01**

Table 10 Neuroimaging measures of the subjects in the study groups.
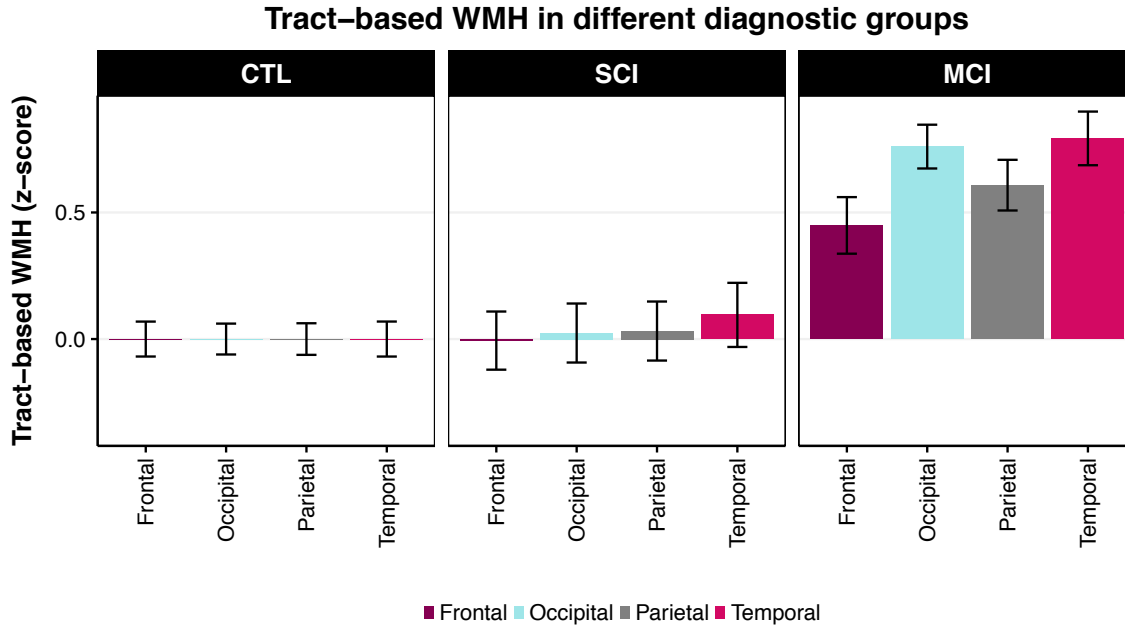
Figure 10 Tract-based White matter hyperintensities in the tracts connected to different gray matter regions.

Tract-based WMH was measured using the steps described in section 3.3.3.4 on all subjects including those subjects used in the creation of the connectivity atlas. In order to visualize the damage in different groups, the z-score of the tract damage measure was calculated for each subject in relation to the control group. Subjects in the CTL group had, by definition, on average zero *tract-based WMH*. SCI subjects had non-significantly higher *tract-based WMH* in all lobes but the damage was only significantly higher in the temporal lobe. MCI subjects had significantly higher *tract-based WMH* in all four lobes, however the damage was more prominent in temporal and occipital lobes (Figure 10).

The fraction of variance in GM volume that is explained by the *tract-based WMH* in tracts connecting to specific regions (e.g. hippocampus volume *vs. tract-based WMH* on tracts connecting to hippocampus) was quantified. In the control group, there were small fractions of variance in the GM volume that could be explained by *tract-based WMH*. The highest fraction of variance explained was observed in the SCI group where the largest explained variances were observed in regions of the temporal and frontal lobe. In the MCI group, the fraction of variance in GM volume explained by the *tract-based WMH* was present, however the fraction of variance explained in the SCI group was much higher. In the MCI group the most prominent explained variance was observed in the temporal lobe (Figure 11).
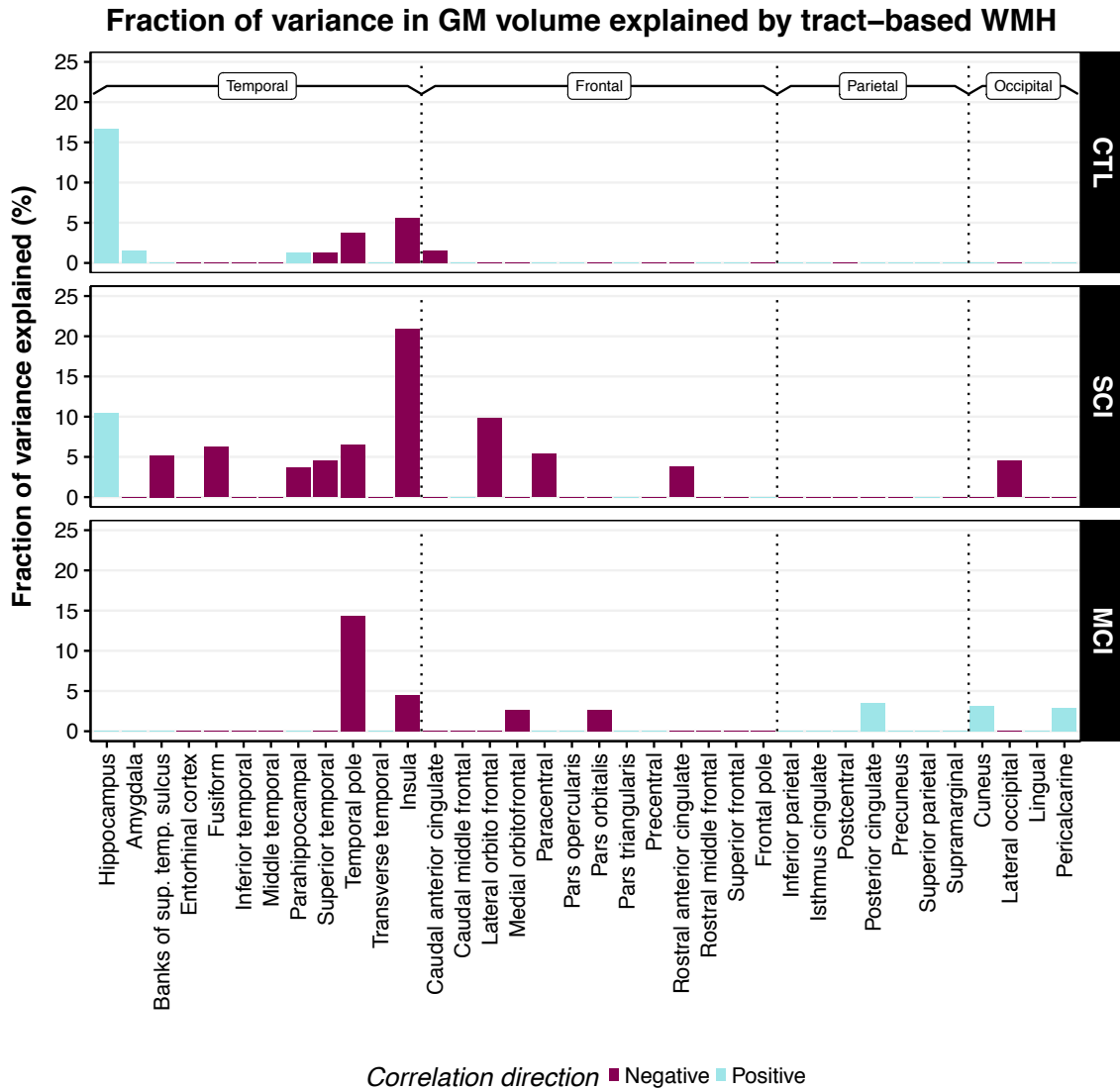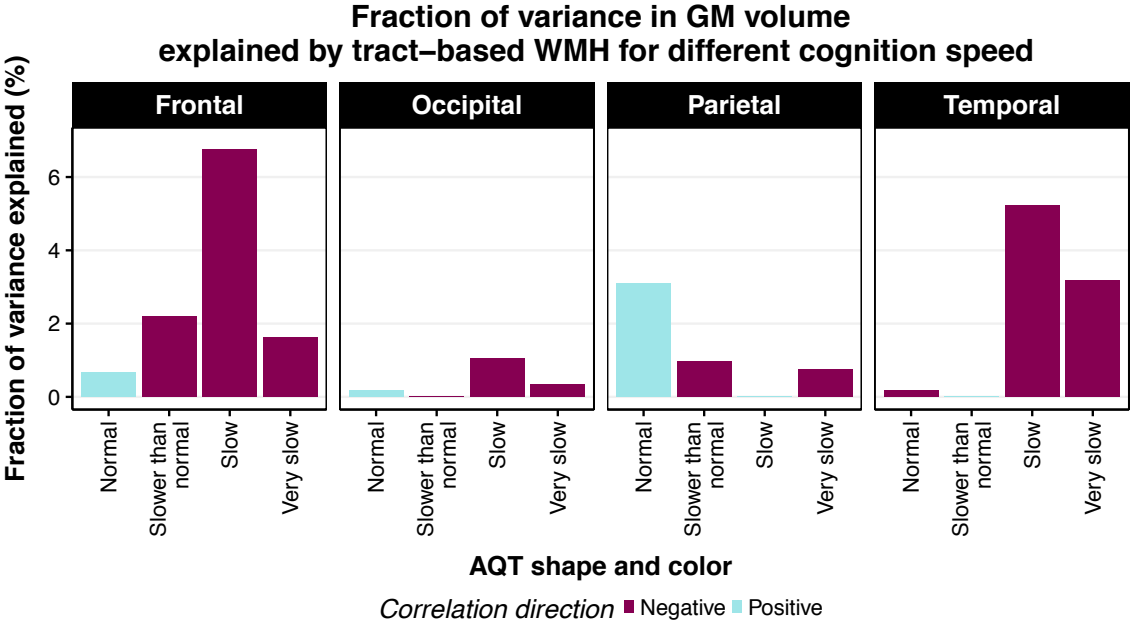
Figure 11 Fraction of variance in the gray matter volume explained by the tract-based white matter hyperintensities in different diagnostic groups.

These results suggested a pattern of effect in each group with the largest effect in the SCI group. In order to assess the same pattern in different levels of cognition speed, the same model was created to measure the variance in GM volume explained by the *tract-based WMH* in the connecting tract but stratifying the subjects by the results of the AQT test instead of their diagnostic groups (Figure 12). Most of the variation in GM volume could be explained by the *tract-based WMH* in subjects with slower than normal (60-70 seconds) and slow (70-90 seconds) compared to the normal (<60 seconds) and very slow (>90 seconds). In particular, the volume of temporal and frontal lobes could be explained by the *tract-based WMH* and the extent of it followed a peaked curved pattern, which was the

same pattern as the one previously observed when analyzing the subjects in CTL, SCI and MCI groups. The patterns however were not present for the parietal lobe and the occipital lobe.

Figure 12 Fraction of variance in the gray matter explained by the tract-based white matter hyperintensities for different levels of cognitive performance.

5 DISCUSSION

5.1 MEASUREMENT OF WHITE MATTER CHANGES

White matter hyperintensities are areas with abnormally high signal intensities on FLAIR or T2-weighted MRI and with low signal intensity on T1-weighted images. This descriptive definition of WMH has been the cornerstone of WMH measurement, both for manual delineations and automatic segmentation. The descriptive definition is subject to interpretation. One can statistically infer the WMH definition using a large sample of manual delineation, however obtaining such a large sample is not easy, if not impossible. So most automatic methods rely on inferring the WMH definition using a small sample and generalizing it using either supervised or unsupervised methods. Therefore, machine-learning methods explicitly or implicitly carry the subjectiveness of the descriptive definition to their results. In order to avoid the use of any explicit or implicit subjectiveness, we attempted to provide a concrete statistical definition of the WMH which implies no human decision. We defined WMH as areas in the WM in which the local image histograms are significantly different from the local histogram of the evidently normal brain on the one-tailed statistical test (3.3.1.3).

Validation of the WMH segmentation using the new proposed definition showed that the definition produces reliable results using any combination of pulse sequences containing either FLAIR or T2 images. Performance of Lesion TOADS [Shiee et al., 2010] and LST [Schmidt et al., 2012], two other available tools for WMH segmentation, was compared to our method, Cascade. WMH volume and Dice coefficient of Cascade was shown to be higher (Figure 7 and Figure 8). The results using the statistical definition were also consistent when different sequences are used independently. This validates that results can be reliably compared or pooled together when using datasets acquired with different image protocols.

The segmentation based on the proposed approach is shown to have marginally better accuracy than other already available methods in the literature and is comparable to manual delineation. However, since the accuracy is measured against the moving target of manual segmentation, accuracy may not be the most crucial performance indicator. One of the main contributions of this thesis is to reformulate the subjective way of WMH definition to an objective one and to show that the WMH segmentation based on the reformulation corresponds well with the manual delineation without implicitly or explicitly relying on it.

The accuracy of the proposed method will be, if not already been, surpassed by other methods relying on the manual delineation in the future. However, the inherent reproducibility of the concrete definition serves a more important role. Until WMH can be directly measured, or we have a sufficiently large and diverse sample to remove the subjectiveness of the classic description of WMH, reproducible methods are favorable to manual delineation.

5.2 CARDIOVASCULAR CONTRIBUTION TO WHITE AND GRAY MATTER CHANGES

The findings of *Study III* confirm the previous evidences of the effect of CHD on regional cortical thickness [Almeida et al., 2008; Koschack and Irle, 2005]. Other cardiovascular comorbidities such as hypertension have also been reported to be associated with smaller GM volume and cortical thickness [Beauchet et al., 2013].

When grouping based on presence or absence of CHD and hypertension, only the group that had both CHD and hypertension had different GM volume and cortical thickness changes compared to the reference group of people without CHD or hypertension. This finding together with the fact that the association between CHD and GM measures remained significant after adjusting for blood pressure (data shown in paper III in the Appendix II), indicates that the effect of CHD on the structural brain changes is in part independent of hypertension.

The data presented in *Study III* did not show any significant association with or difference in the WMH volume in groups with and without CHD and hypertension. Although the idea of the effect of cardiovascular diseases on WMH volume seems plausible, other studies specially those focusing on early signs of changes, have also failed to observe such an effect [Maillard et al., 2012]. We believe that failing to observe such an effect in early stages is rooted in the fact that the total WMH volume is too crude a measure to be able to capture disease-related changes. *Study IV*, where the WMH were measured per tract and showed significant disease related changes, supports the idea that the WMH needs to be measured while taking their location into account.

5.3 WHITE AND GRAY MATTER CHANGES IN COGNITIVE IMPAIRMENT

Study IV shows that the crude burden of WMH is higher in subjects with MCI compared to CTL and SCI. CTL subjects had the least load and SCI subjects had non-significantly higher levels of damage, while MCI subjects showed significantly higher levels of tract damage (Figure 10). Although the way we measured WMH damage was different, these

results validate previous findings [Appelros et al., 2005; Debette et al., 2007; Dufouil et al., 2009; Jokinen et al., 2009].

The main finding of this thesis is that the relation between the damage due to WMH and atrophy in the anatomically connected GM region is strongest in the subjects with SCI when compared to both CTL and MCI subjects. Similarly, when grouping the subjects into groups with different cognitive speed, based on the AQT test and regardless of their diagnosis, there was little variation in GM that can be explained by *tract-based WMH* in subjects with high cognitive performance (i.e. fast AQT) and for subjects with high cognitive impairment (i.e. very slow AQT). The explained variation was however highest in subjects with subtle cognitive impairment. Both these patterns of explained variance point to the fact that the effect of *tract-based WMH* on the GM atrophy in the connecting region is highest in the early stage of cognitive impairment in subjects that are between the pre-clinical and the SCI phase of the disease.

The small variance in GM volume change explained by the *tract-based WMH* in subjects who are still cognitively normal can be due to subtle changes in the GM at the very early stages (Figure 13). GM changes are known to have larger variation in cognitively impaired subjects (MCI and SCI) [Jack et al., 2013]. This can certify why the explained variation is high in SCI subjects as well as in subjects with medium AQT results. The low explained variance in GM atrophy by the *tract-based WMH* in connecting tracts should be either (a) due to small changes in the damage (i.e. plateau effect) or (b) due to the lack of association between them. Since the association is very strong for SCI subjects and subjects with medium AQT results it seems less likely that the lack of association is the reason and thus the plateau effect is the most likely explanation.

The low relation between GM atrophy and *tract-based WMH* in MCI subjects and subjects with slow AQT results is the most significant result of the thesis. It suggests the amount of atrophy explained by tract damage may reach a plateau. An explanation could be that the damage in the white matter precedes the GM atrophy (Figure 13-A). Previous neuroimaging studies [Iadecola, 2004; Iturria-Medina et al., 2016; Zlokovic, 2011] and epidemiological studies that show WMH or its risk factor can predict cognitive decline down the road [Vermeer et al., 2003] may support this hypothesis. Another explanation could be that, the presence of coexistent pathology in MCI subjects could cloud the relation between local GM atrophy and *tract-based WMH* [van Westen et al., 2016]. This could

mean that the development of WM tract damage is not independent and secondary to GM atrophy and just contributes to the clinical manifestation of the disease (Figure 13-B).

In reality, both interpretations are probably correct to some extent. The first interpretation is more plausible for subjects who are more susceptible to WM damage, namely those with high cardiovascular burden. For these subjects, the WM pathology injures axons and axonal injury subsequently triggers the nerve cell death which manifests as the GM degeneration (i.e. Wallerian-like degeneration). The second interpretation is reasonable for subjects with more AD-like pathology. For these subjects WMH plays an additive role and amplifies the clinical manifestation of pathologies. We cannot however prove or disprove this explanation with the present data; both hypotheses can be tested when reproducing the above results in Aβ positive and negative subgroups with and without cardiovascular risk factors. Although temporal precedence or statistical causation of GM and WM change can be estimated using advanced statistical models, using longitudinal data is the ultimate way to test these two hypotheses.
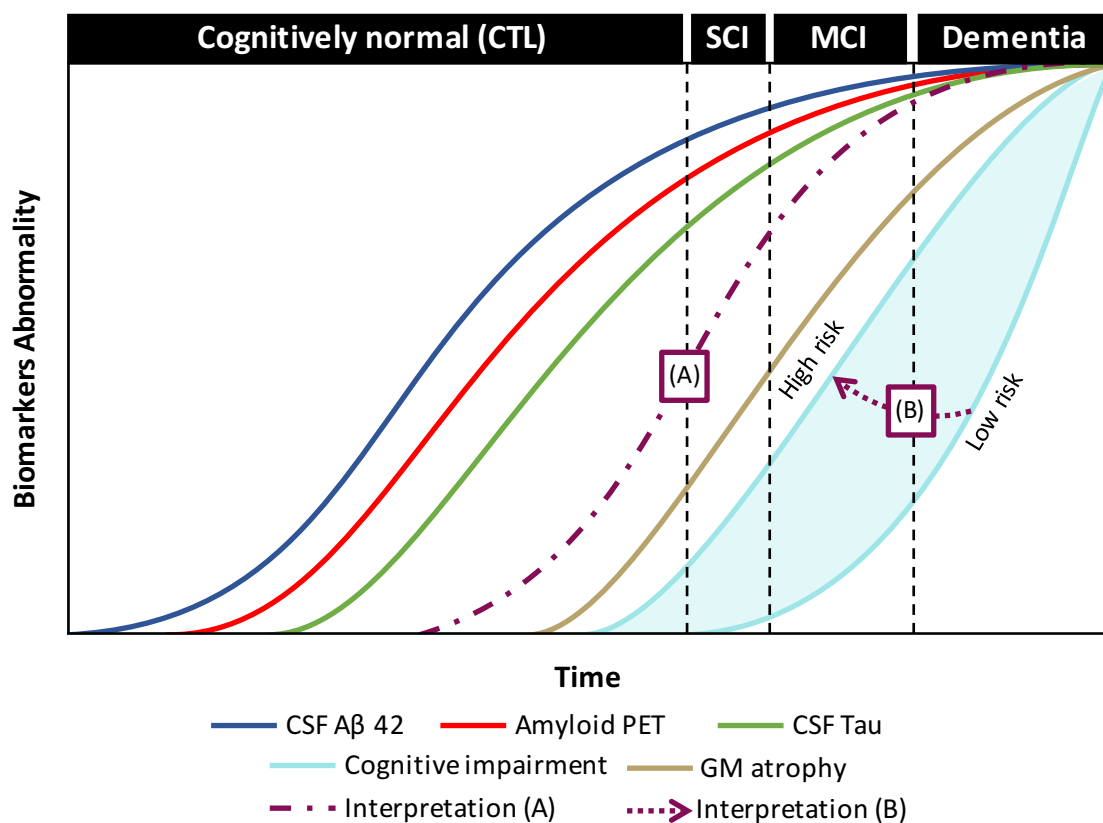
Figure 13 Possible interpretations of the high fraction of variance in gray matter atrophy explained by tract-based WMH observed in subject with subtle cognitive impairment. (A) Tract-based WMH might proceed GM atrophy (B) Tract-based WMH only amplify the clinical manifestation.

6 CONCLUSION

The main aims of this thesis were (1) to develop and validate an automatic method for the segmentation of WMH that can be employed in different research settings and (2) to investigate the role of WMH in early stages of cognitive impairment.

In *Study I* and *Study II*, we developed a fast and flexible automatic WMH segmentation method, capable of using different MRI input sequences. We proposed a new statistical definition for the WMH to remove any implicit or explicit need for manually delineated WMH as reference and showed the resulting segmentation has high reproducibility and accuracy. The method is implemented as an open-source software available at https://github.com/Damangir/Cascade.

Study III investigated the relation between CHD and hypertension and cortical thickness, GM volume and WMH. Associations between CHD, cortical thickness and GM volume were strongest in people with both CHD and hypertension in midlife. No association was found between CHD and WML volumes which was probably due to measuring WMH as absolute volume which is too crude a measure. Our further investigation in *Study IV* showed that the role of WMH is more pronounced when its burden is measured on a per tract basis. The *tract-based WMH* was higher in subjects with more cognitive impairment even early in the disease. CTL had the least damage and SCI subjects had non-significantly higher levels of tract damage, while MCI subjects showed significantly higher levels of tract damage. *Tract-based WMH* also explained more variation in the volume of GM connected through the tract in SCI subjects compared to both CTL and MCI subjects which suggests that WMH plays a more important role in the early stages of cognitive impairment.

In conclusion, our results showed that WMH is not a mere incidental finding and is instead an important aspect of the disease development. The spatial patterns of WMH and in particular *tract-based WMH* have a potential of being used as biomarkers in the future.

7 FUTURE WORK

The methods developed in the thesis for measuring WMH allowed the detailed analysis of WMH and the tracts affected by them. Given more time in the future, the methods should evolve to mature software to be usable even by a larger community.

Moreover, the presence of WMH per se can undermine current image processing algorithms. Although the effect of WMH is minimized in the developed methods, different parts of the methods need to be validated independently in the presence of WMH. In particular, one needs to measure the effect of WMH on:

- Registration, inhomogeneity correction and brain tissue segmentation in *Study I* and *Study II*
- Registration and GM parcellation in *Study III* and *Study VI*

The results presented in *Study VI* also urge the investigation of the same effect in a longitudinal study. The effect of cardiovascular risk factors and AD pathology biomarkers such as Aβ, measured in CSF and through PET amyloid imaging, needs to be studied as well. Given those data one may be able distinguish subjects in whom WM damage precedes the GM changes from those in which WM damage follows the GM change.

Moreover, having known the results presented in *Study VI*, one might apply the same method to the data in *Study III* to study whether detailed measurements of WMH can have an association with CHD and hypertension.

Finally, in order for other researchers to be able to build upon the current knowledge and experience, material and methods should be as openly available as possible. To this end, all developed methods in this thesis are made public in the hope that all researchers realize that they will indeed gain more by making their materials openly accessible.

8 ACKNOWLEDGEMENTS

9 REFERENCES

Dag Aarsland, Arvid Rongve, Sabine Piepenstock Nore, Ragnhild Skogseth, Siri Skulstad, Uwe Ehrt, Dagne Hoprekstad, and Clive Ballard, 2008. Frequency and case identification of dementia with Lewy bodies using the revised consensus criteria. Dement. Geriatr. Cogn. Disord. 26, 445–452.

Marilyn S. Albert, Steven T. DeKosky, Dennis Dickson, Bruno Dubois, Howard H. Feldman, Nick C. Fox, Anthony Gamst, David M. Holtzman, William J. Jagust, Ronald C. Petersen, Peter J. Snyder, Maria C. Carrillo, Bill Thies, and Creighton H. Phelps, 2011. The diagnosis of mild cognitive impairment due to Alzheimer's disease: Recommendations from the National Institute on Aging-Alzheimer's Association workgroups on diagnostic guidelines for Alzheimer's disease. Alzheimer's Dement. J. Alzheimer's Assoc. 7, 270–279.

Osvaldo P. Almeida, Griselda J. Garrido, Christopher Beer, Nicola T. Lautenschlager, Leonard Arnolda, Nat Lenzo, Andrew Campbell, and Leon Flicker, 2008. Coronary heart disease is associated with regional grey matter volume loss: implications for cognitive function and behaviour. Intern. Med. J. 38, 599–606.

American Psychiatric Association, 1994. Diagnostic and Statistical Manual of Mental Disorders: DSM-IV., Diagnostic and Statistical Manual of Mental Disorders. American Psychiatric Association.

Peter Appelros, Margareta Samuelsson, and Dan Lindell, 2005. Lacunar infarcts: Functional and cognitive outcomes at five years in relation to MRI findings. Cerebrovasc. Dis. 20, 34–40.

Lars Bäckman, Sari Jones, Anna-Karin Berger, Erika Jonsson Laukka, and Brent J. Small, 2005. Cognitive impairment in preclinical Alzheimer's disease: a meta-analysis. Neuropsychology 4, 520–531.

Olivier Beauchet, Sébastien Celle, Frédéric Roche, Robert Bartha, Manuel Montero-Odasso, Gilles Allali, and Cédric Annweiler, 2013. Blood pressure levels and brain volume reduction: a systematic review and meta-analysis. J. Hypertens. 31, 1502–1516.

Timothy E.J. Behrens, Mark W. Woolrich, Mark Jenkinson, Heidi Johansen-Berg, Rita G. Nunes, Stuart Clare, Paul M. Matthews, Michael Brady, and Stephen M. Smith, 2003.

Characterization and Propagation of Uncertainty in Diffusion-Weighted MR Imaging. Magn. Reson. Med. 50, 1077–1088.

Jean-François Buyck, Carole Dufouil, Bernard Mazoyer, Pauline Maillard, Pierre Ducimetière, Annick Alpérovitch, Marie-Germaine Bousser, Tobias Kurth, and Christophe Tzourio, 2009. Cerebral white matter lesions are associated with the risk of stroke but not with other vascular events: the 3-City Dijon Study. Stroke 40, 2327–2331.

Charles Edward Coffey, Gary S. Figiel, William T. Djang, William B. Saunders, and Richard D. Weiner, 1989. White matter hyperintensity on magnetic resonance imaging: clinical and neuroanatomic correlates in the depressed elderly. J. Neuropsychiatry Clin. Neurosci. 1, 135–144.

Stéphanie Debette, Alexa Beiser, Charles S. DeCarli, Rhoda Au, Jayandra J. Himali, Margaret Kelly-Hayes, Jose R. Romero, Carlos S. Kase, Philip A. Wolf, and Sudha Seshadri, 2010. Association of MRI Markers of Vascular Brain Injury With Incident Stroke, Mild Cognitive Impairment, Dementia, and Mortality. Stroke 41, 600–606.

Stéphanie Debette, Stéphanie Bombois, Amélie Bruandet, Xavier Delbeuck, Samuel Lepoittevin, Christine Delmaire, Didier Leys, and Florence Pasquier, 2007. Subcortical hyperintensities are associated with cognitive decline in patients with mild cognitive impairment. Stroke 38, 2924–2930.

Lee R. Dice, 1945. Measures of the Amount of Ecologic Association Between Species. Ecology 26, 297–302.

Carole Dufouil, Ophélia Godin, John Chalmers, Oghuzan Coskun, Stephen MacMahon, Nathalie Tzourio-Mazoyer, Marie-Germaine Bousser, Craig Anderson, Bernard Mazoyer, and Christophe Tzourio, 2009. Severe cerebral white matter hyperintensities predict severe cognitive decline in patients with cerebrovascular disease history. Stroke.

Farshad Falahati, Seyed-Mohammad Fereshtehnejad, Dorota Religa, Lars-Olof Wahlund, Eric Westman, and Maria Eriksdotter, 2015. The use of MRI, CT and lumbar puncture in dementia diagnostics: data from the SveDem Registry. Dement. Geriatr. Cogn. Disord. 39, 81–91.

Franz Fazekas, John B. Chawluk, and Abass Alavi, 1987. MR signal abnormalities at 1.5 T in Alzheimer's dementia and normal aging. Am. J. Roentgenol. 149, 351–356.

Ellen Garde, Erik Lykke Mortensen, Katja Krabbe, Egill Rostrup, and Henrik B.W. Larsson, 2000. Relation between age-related decline in intelligence and cerebral white-matter hyperintensities in healthy octogenarians: a longitudinal study. Lancet 356, 628–634.

Alida A. Gouw, Wiesje Maria van der Flier, Elisabeth C.W. van Straaten, Leonardo Pantoni, Antonio J. Bastos-Leite, Domenico Inzitari, Timo Erkinjuntti, Lars-Olof Wahlund, C. Ryberg, Reinhold Schmidt, Franz Fazekas, Philip Scheltens, and Frederik Barkhof, 2008. Reliability and sensitivity of visual scales versus volumetry for evaluating white matter hyperintensity progression. Cerebrovasc. Dis. 25, 247–253.

Mahmut Edip Gurol, Michael C. Irizarry, Eric E. Smith, Susan Raju, Ramon Diaz-Arrastia, Teodoro Bottiglieri, Jonathan Rosand, John H. Growdon, and Steven M. Greenberg, 2006. Plasma β-amyloid and white matter lesions in AD, MCI, and cerebral amyloid angiopathy. Neurology 66, 23–29.

Richard J. Havlik, Daniel J. Foley, Bryan Sayer, Kamal Masaki, Lon White, and Lenore J. Launer, 2002. Variability in Midlife Systolic Blood Pressure Is Related to Late-Life Brain White Matter Lesions. Stroke 33, 26–30.

Christopher M. Holland, Eric E. Smith, Istvan Csapo, Mahmut Edip Gurol, Douglas A. Brylka, Ronald J. Killiany, Deborah Blacker, Marilyn S. Albert, Charles R.G. Guttmann, and Steven M. Greenberg, 2008. Spatial Distribution of White-Matter Hyperintensities in Alzheimer Disease, Cerebral Amyloid Angiopathy, and Healthy Aging. Stroke 39, 1127–1133.

Costantino Iadecola, 2004. Neurovascular regulation in the normal brain and in Alzheimer's disease. Nat Rev Neurosci 5, 347–360.

Yasser Iturria-Medina, Roberto C. Sotero, Paule J. Toussaint, José María Mateos-Pérez, Alan C. Evans, and The Alzheimer's Disease Neuroimaging Initiative, 2016. Early role of vascular dysregulation on late-onset Alzheimer's disease based on multifactorial data-driven analysis. Nat. Commun. 7, 1–14.

Clifford R. Jack, David S. Knopman, William J. Jagust, Ronald C. Petersen, Michael W. Weiner, Paul S. Aisen, Leslie M. Shaw, Prashanthi Vemuri, Heather J. Wiste, Stephen D. Weigand, Timothy G. Lesnick, Vernon S. Pankratz, Michael C. Donohue, and John Q. Trojanowski, 2013. Tracking pathophysiological processes in Alzheimer's disease: an updated hypothetical model of dynamic biomarkers. Lancet Neurol. 12, 207–216.

Clifford R. Jack, David S. Knopman, William J. Jagust, Leslie M. Shaw, Paul S. Aisen, Michael W. Weiner, Ronald C. Petersen, and John Q. Trojanowski, 2010. Hypothetical model of dynamic biomarkers of the Alzheimer's pathological cascade. Lancet Neurol. 9, 119–128.

Mark Jenkinson, and Stephen M. Smith, 2001. A global optimisation method for robust affine registration of brain images. Med. Image Anal. 5, 143–156.

Hanna Jokinen, Hely Kalska, Raija Ylikoski, Sofia Madureira, Ana Verdelho, Wiesje Maria Van der Flier, Philip Scheltens, Frederik Barkhof, Marieke C. Visser, Franz Fazekas, Reinhold Schmidt, John T. O'Brien, Gunhild Waldemar, Anders Wallin, Hugues Chabriat, Leonardo Pantoni, Domenico Inzitari, and Timo Erkinjuntti, 2009. Longitudinal cognitive decline in subcortical ischemic vascular disease -the ladis study. Cerebrovasc. Dis. 27, 384–391.

Janka Koschack, and Eva Irle, 2005. Small hippocampal size in cognitively normal subjects with coronary artery disease. Neurobiol. Aging 26, 865–871.

Gabor G. Kovacs, Ivan Milenkovic, Adelheid Wöhrer, Romana Höftberger, Ellen Gelpi, Christine Haberler, Selma Hönigschnabl, Angelika Reiner-Concin, Harald Heinzl, Susanne Jungwirth, Wolfgang Krampla, Peter Fischer, and Herbert Budka, 2013. Non-Alzheimer neurodegenerative pathologies and their combinations are more frequent than commonly believed in the elderly brain: a community-based autopsy series. Acta Neuropathol. 126, 365–384.

Duanping Liao, Lawton Cooper, Jianwen Cai, James F. Toole, Nick R. Bryan, Gregory L. Burke, Eyal Shahar, Javier Nieto, Thomas H. Mosley, and Gerardo Heiss, 1997. The prevalence and severity of white matter lesions, their relationship with age, ethnicity, gender, and cardiovascular disease risk factors: the ARIC Study. Neuroepidemiology. 16, 149–162.

Lonnie Magee, 1990. R 2 Measures Based on Wald and Likelihood Ratio Joint Significance Tests. Am. Stat. 44, 250–253.

Pauline Maillard, Sudha Seshadri, Alexa Beiser, Jayandra J. Himali, Rhoda Au, Evan Fletcher, Owen Carmichael, Philip A. Wolf, and Charles S. DeCarli, 2012. Effects of systolic blood pressure on white-matter integrity in young adults in the Framingham Heart Study: a cross-sectional study. Lancet Neurol. 11, 1039–1047.

Teri A. Manolio, Gregory L. Burke, Daniel H. O'Leary, Gregory Evans, Norman

Beauchamp, Laurie Knepper, and Beverly Ward, 1999. Relationships of Cerebral MRI Findings to Ultrasonographic Carotid Atherosclerosis in Older Adults. Arterioscler. Thromb. Vasc. Biol. 19, 356–365.

Natalie L. Marchant, Bruce R. Reed, Charles S. DeCarli, Cindee M. Madison, Michael W. Weiner, Helena C. Chui, and William J. Jagust, 2012. Cerebrovascular disease, beta-amyloid, and cognition in aging. Neurobiol. Aging 33, 1006.e25-1006.e36.

Guy M. McKhann, David S. Knopman, Howard Chertkow, Bradley T. Hyman, Clifford R. Jack, Claudia H. Kawas, William E. Klunk, Walter J. Koroshetz, Jennifer J. Manly, Richard Mayeux, Richard C. Mohs, John C. Morris, Martin N. Rossor, Philip Scheltens, Maria C. Carrillo, Bill Thies, Sandra Weintraub, and Creighton H. Phelps, 2011. The diagnosis of dementia due to Alzheimer's disease: Recommendations from the National Institute on Aging-Alzheimer's Association workgroups on diagnostic guidelines for Alzheimer's disease. Alzheimer's Dement. 7, 263–269.

Organisation for Economic Co-operation and Development, 2016. OECD Data [WWW Document]. 2016. URL https://data.oecd.org/gdp/gross-domestic-product-gdp.htm (accessed 2.3.17).

Leonardo Pantoni, Michela Simoni, Giovanni Pracucci, Reinhold Schmidt, Frederik Barkhof, and Domenico Inzitari, 2002. Visual Rating Scales for Age-Related White Matter Changes (Leukoaraiosis). Stroke 33, 2827–2833.

Ronald C. Petersen, Glenn E. Smith, Stephen C. Waring, Robert J. Ivnik, Eric George Tangalos, and Emre Kokmen, 1999. Mild cognitive impairment: clinical characterization and outcome. Arch. Neurol. 56, 303–308.

Niels D. Prins, Ewoud J. van Dijk, Tom den Heijer, Sarah E. Vermeer, Jellemer Jolles, Peter J. Koudstaal, Albert Hofman, and Monique M.B. Breteler, 2005. Cerebral small-vessel disease and decline in information processing speed, executive function and memory. Brain 128, 2034–2041.

Parnesh Raniga, Pierre Schmitt, Pierrick Bourgeat, Jurgen Fripp, Victor L. Villemagne, Christopher C. Rowe, and Olivier Salvado, 2011. Local intensity model: An outlier detection framework with applications to white matter hyperintensity segmentation, in: 2011 IEEE International Symposium on Biomedical Imaging: From Nano to Macro. IEEE, pp. 2057–2060.

Dorota Religa, Seyed-Mohammad Fereshtehnejad, Pavla Cermakova, Ann-Katrin Edlund,

Sara Garcia-Ptacek, Nicklas Granqvist, Anne Hallbäck, Kerstin Kåwe, Bahman Farahmand, Lena Kilander, Ulla-Britt Mattsson, Katarina Nägga, Peter Nordström, Helle Wijk, Anders Wimo, Bengt Winblad, and Maria Eriksdotter, 2015. SveDem, the Swedish Dementia Registry – A Tool for Improving the Quality of Diagnostics, Treatment and Care of Dementia Patients in Clinical Practice. PLoS One 10, 1–14.

Philip Scheltens, Frederik Barkhof, Didier Leys, Jean Pierre Pruvo, Jozef J. Nauta, Pierre Vermersch, Marc Steinling, and Jaap Valk, 1993. A semiquantative rating scale for the assessment of signal hyperintensities on magnetic resonance imaging. J. Neurol. Sci. 114, 7–12.

Philip Scheltens, Timo Erkinjuntti, Didier Leys, Lars-Olof Wahlund, Domenico Inzitari, Teodoro del Ser, Florence Pasquier, Frederik Barkhof, Riita Mäntylä, John V. Bowler, Anders Wallin, Joseph A. Ghika, Franz Fazekas, and Leonardo Pantoni, 1998. White matter changes on CT and MRI: an overview of visual rating scales. European Task Force on Age-Related White Matter Changes. Eur. Neurol. 39, 80–89.

Paul Schmidt, Christian Gaser, Milan Arsic, Dorothea Buck, Annette Förschler, Achim Berthele, Muna Hoshi, Rüdiger Ilg, Volker J. Schmid, Claus Zimmer, Bernhard Hemmer, and Mark Mühlau, 2012. An automated tool for detection of FLAIR-hyperintense white-matter lesions in multiple sclerosis. Neuroimage 59, 3774–3783.

Reinhold Schmidt, Christian Enzinger, Stefan Ropele, Helena Schmidt, and Franz Fazekas, 2003. Progression of cerebral white matter lesions: 6-year results of the Austrian Stroke Prevention Study. Lancet 361, 2046–2048.

Bernhard Schölkopf, Stefanie Mika, Christopher J.C. Burges, Peter Knirsch, Klaus-Robert Müller, Gunnar Rätsch, and Alex J. Smola, 1999. Input space versus feature space in kernel-based methods. IEEE Trans. neural networks 10, 1000–1017.

Navid Shiee, Pierre-Louis PL Bazin, Arzu Ozturk, Daniel S. Reich, Peter A. Calabresi, and Dzung L. Pham, 2010. A topology-preserving approach to the segmentation of brain images with multiple sclerosis lesions. Neuroimage 49, 1524–1535.

Andrew Simmons, Eric Westman, J. Sebastian Muehlboeck, Patrizia Mecocci, Bruno Vellas, Magda Tsolaki, Iwona Kłoszewska, Lars-Olof Wahlund, Hilkka Soininen, Simon Lovestone, Alan C. Evans, and Christian Spenger, 2011. The AddNeuroMed framework for multi-centre MRI assessment of Alzheimer's disease: experience from the first 24 months. Int. J. Geriatr. Psychiatry 26, 75–82.

John G. Sled, Alex P. Zijdenbos, and Alan C. Evans, 1998. A nonparametric method for automatic correction of intensity nonuniformity in MRI data. IEEE Trans. Med. Imaging 17, 87–97.

Stephen M. Smith, 2002. Fast robust automated brain extraction. Hum. Brain Mapp. 17, 143–155.

Socialstyrelsen, 2014. Demenssjukdomarnas samhällskostnader i Sverige 2012.

Martijn D. Steenwijk, Petra J.W. Pouwels, Marita Daams, Jan Willem van Dalen, Matthan W.A. Caan, Edo Richard, Frederik Barkhof, and Hugo Vrenken, 2013. Accurate white matter lesion segmentation by k nearest neighbor classification with tissue type priors (kNN-TTPs). NeuroImage Clin. 3, 462–469.

Kyle Strimbu, and Jorge A. Tavel, 2010. What are biomarkers? Curr. Opin. HIV AIDS 5, 463–466.

Alexander N.W. Taylor, Lana Kambeitz-Ilankovic, Benno Gesierich, Lee Simon-Vermot, Nicolai Franzmeier, Miguel Á. Araque Caballero, Sophia Müller, Liu Hesheng, Birgit Ertl-Wagner, Katharina Bürger, Michael W. Weiner, Martin Dichgans, Marco Duering, and Michael Ewers, 2017. Tract-specific white matter hyperintensities disrupt neural network function in Alzheimer's disease. Alzheimer's Dement. 13, 225–235.

Mats Tullberg, Evan Fletcher, Charles S. DeCarli, Dan Mungas, Bruce R. Reed, Danielle J. Harvey, Michael W. Weiner, Helena C. Chui, and William J. Jagust, 2004. White matter lesions impair frontal lobe function regardless of their location. Neurology 63, 246–253.

Ewoud J. van Dijk, Monique M.B. Breteler, Reinhold Schmidt, Klaus Berger, Lars-Göran Nilsson, Matthijs Oudkerk, Andrzej Pajak, Susana Sans, Maria de Ridder, Carole Dufouil, Rebecca Fuhrer, Simona Giampaoli, Lenore J. Launer, and Albert Hofman, 2004. The Association Between Blood Pressure, Hypertension, and Cerebral White Matter Lesions. Hypertension 44, 625–630.

Elisabeth C.W. van Straaten, Franz Fazekas, Egill Rostrup, Philip Scheltens, Reinhold Schmidt, Leonardo Pantoni, Domenico Inzitari, Gunhild Waldemar, Timo Erkinjuntti, Riita Mäntylä, Lars-Olof Wahlund, and Frederik Barkhof, 2006. Impact of white matter hyperintensities scoring method on correlations with clinical data: The LADIS study. Stroke 37, 836–840.

Danielle van Westen, Daniel Lindqvist, Kaj Blennow, Lennart Minthon, Katarina Nägga, Erik Stomrud, Henrik Zetterberg, and Oskar Hansson, 2016. Cerebral white matter lesions – associations with Aβ isoforms and amyloid PET. Sci. Rep. 6, 1–9.

Sarah E. Vermeer, Niels D. Prins, Tom den Heijer, Albert Hofman, Peter J. Koudstaal, and Monique M.B. Breteler, 2003. Silent Brain Infarcts and the Risk of Dementia and Cognitive Decline. N. Engl. J. Med. 348, 1215–1222.

Lars-Olof Wahlund, Frederik Barkhof, Franz Fazekas, Lena Bronge, Michael Augustin, Magnus Sjogren, Anders Wallin, Herman Adèr, Didier Leys, Leonardo Pantoni, Florence Pasquier, Timo Erkinjuntti, and Philip Scheltens, 2001. A New Rating Scale for Age-Related White Matter Changes Applicable to MRI and CT. Stroke 32, 1318–1322.

Lon White, Brent J. Small, Helen Petrovitch, G. Webster Ross, Kamal Masaki, Robert D. Abbott, John Hardman, Daron Davis, James Nelson, and William Markesbery, 2005. Recent Clinical-Pathologic Research on the Causes of Dementia in Late Life: Update From the Honolulu-Asia Aging Study. J. Geriatr. Psychiatry Neurol. 18, 224–227.

Anders Wimo, Maëlenn Guerchet, Gemma-Claire Ali, Yu-Tzu Wu, A. Matthew Prina, Bengt Winblad, Linus Jönsson, Zhaorui Liu, and Martin Prince, 2017. The worldwide costs of dementia 2015 and comparisons with 2010. Alzheimer's Dement. 13, 1–7.

Anders Wimo, Linus Jönsson, Laura Fratiglioni, Per Olof Sandman, Anders Gustavsson, Anders Sköldunger, and Lennarth Johansson, 2016. The societal costs of dementia in Sweden 2012 - relevance and methodological challenges in valuing informal care. Alzheimers. Res. Ther. 8, 1–11.

Ari Ylikoski, Timo Erkinjuntti, Raili Raininko, Seppo Sarna, Raimo Sulkava, and Reijo Tilvis, 1995. White Matter Hyperintensities on MRI in the Neurologically Nondiseased Elderly. Stroke 26, 1171–1177.

Yongyue Zhang, Michael Brady, and Stephen M. Smith, 2001. Segmentation of brain MR images through a hidden Markov random field model and the expectation-maximization algorithm. IEEE Trans. Med. Imaging 20, 45–57.

Yongxia Zhou, Fang Yu, Timothy Q. Duong, and for the Alzheimer's Disease Neuroimaging Initiative, 2015. White matter lesion load is associated with resting state functional MRI activity and amyloid pet but not FDG in mild cognitive impairment and early alzheimer's disease patients. J. Magn. Reson. Imaging 41, 102–109.

Hongwei Zhu, and Otman Basir, 2003. Automated brain tissue segmentation and MS lesion detection using fuzzy and evidential reasoning, in: Proceedings of the IEEE International Conference on Electronics, Circuits, and Systems. pp. 1070–1073.

Alex P. Zijdenbos, Reza Forghani, and Alan C. Evans, 2002. Automatic "pipeline" analysis of 3-D MRI data for clinical trials: application to multiple sclerosis. IEEE Trans. Med. Imaging 21, 1280–1291.

Berislav V Zlokovic, 2011. Neurovascular pathways to neurodegeneration in Alzheimer's disease and other disorders. Nat Rev Neurosci 12, 723–738.

10 APPENDIX 1: EXTERNAL SOFTWARES

10.1 FREESURFER SOFTWARE SUITE

FreeSurfer is an open-source software package by the Laboratory for Computational Neuroimaging at the Athinoula A. Martinos Center for Biomedical Imaging for analyzing structural and functional neuroimaging data.

We used FreeSurfer for analyzing structural MRI. The process starts with pre-processing including motion correction, brain tissue extraction, registration to the Talairach space, segmentation of the subcortical WM and deep GM volumetric structures, intensity normalization. Next the GM/WM boundary is created as a 3D mesh followed by topological matching of the boundaries before deforming the boundaries to match the highest intensity gradient and form the cortical model. After the cortical models are complete, the model surface is inflated and then registered to a spherical atlas. Then cortical parcellation is performed to segment gyral and sulcal structures, from which cortical thickness is measured as the closest distance from the GM/WM boundary to the GM/CSF boundary at each vertex on the meshed surface. Since a high-resolution mesh reconstruction is performed, the cortical thickness measures are not restricted to the voxel resolution of the original image and thus are capable of detecting subtle group differences. Detail description as well as access to the software suite is available at https://surfer.nmr.mgh.harvard.edu/.

10.2 CIVET PIPELINE

CIVET is a web-based tool developed at the McConnell Brain Imaging Centre of the Montreal Neurological Institute, McGill University. It is an image processing pipeline for fully automated cortical measurements, morphometric and volumetric analyses of MRI images of human brain.

CIVET starts by an affine transformation of the MR images from native to the MNI standard space. The registered images are then corrected for inhomogeneity before extracting brain from them. A non-linear transformation is then computed from the subject to the MNI standard space. Then CIVET continues by classifying the brain tissue into WM, GM, and CSF. Thereafter the brain is divided into two hemispheres before proceeding to surface extraction.

White matter surface is modeled as the boundary between cortical GM and subcortical WM using a mesh of 40,962 vertices and 81,920 faces. The GM surface is then calculated by expanding outwards from the WM surface toward the CSF. The surfaces are then

transformed into the MNI standard surface template in order to allow group comparisons. The cortical thickness is then calculated as the distance between the WM and GM surfaces in the original native space. Detailed description and the web-platform itself is available at http://www.bic.mni.mcgill.ca/ServicesSoftware/CIVET.

11 APPENDIX 2: CONSTITUENT PAPERS

I. **Soheil Damangir**, Amirhossein Manzouri, Ketil Oppedal, Stefan Carlsson, Michael J. Firbank, Hogne Sonnesyn, Ole-Bjørn Tysnes, John T. O'Brien, Mona K. Beyer, Eric Westman, Dag Aarsland, Lars-Olof Wahlund, and Gabriela Spulber, 2012. Multispectral MRI segmentation of age related white matter changes using a cascade of support vector machines. J. Neurol. Sci. 322, 211–216.

II. **Soheil Damangir**, Eric Westman, Andrew Simmons, Hugo Vrenken, Lars-Olof Wahlund, and Gabriela Spulber, 2016. Reproducible Segmentation of White Matter Hyperintensities Using a New Statistical Definition. Magn. Reson. Mater. Physics, Biol. Med. 30, 227–237.

III. Miika Vuorinen, **Soheil Damangir**, Eini Niskanen, Julia Miralbell, Minna Rusanen, Gabriela Spulber, Hilkka Soininen, Miia Kivipelto, and Alina Solomon, 2014. Coronary heart disease and cortical thickness, gray matter and white matter lesion volumes on MRI. PLoS One 9, 1–9.

IV. **Soheil Damangir**, Oskar Hansson, Olof Lindberg, Erik Stomrud, Danielle van Westen, Eric Westman, Hugo Vrenken, Lars-Olof Wahlund and Gabriela Spulber. 2017. The relationship between gray matter atrophy and white matter hyperintensities in anatomically connected tracts in subjects with cognitive impairment. Submitted manuscript

All previously published papers were reproduced with permission from the publisher.